Department of Signal Processing and Acoustics

KAPRI Final Report

The Finnish Work Environment Fund Project no. 111244

Sami Oksanen

KAPRI Final Report

The Finnish Work Environment Fund Project no. 111244

Sami Oksanen

NORDIC ECOLABEL

441   697
Printed matter

Author

Sami Oksanen

Abstract

This report summarizes the results of the KAPRI project, noise generation mechanisms of the percussive rock drilling and breaking hammer operations. At first, a literature study was conducted to find out existing knowledge on the topic. The literature study was mainly focused on the stress wave analysis and modeling of drilling equipment. Based on the findings of the literature study a brief theoretical introduction was written.

The theory was tested in practice by conducting a series of strain wave, acoustic, and surface vibrations measurements under laboratory conditions. To gain more understanding on the vibration phenomena in drill steels computational models were developed to provide tools for the sound production modeling of the drill steels.

The modeling approach was to utilize modeling techniques that have previously been used in musical instrument modeling, such as digital waveguides and dispersion filters. The modeling process was divided to two main approaches namely a longitudinal stress wave model and a transversal stress wave model that is used in modeling of the majority of the sound output generated in drilling. The research work in the project had also a separate minor research topic namely acoustical analysis of excavated tunnels in rock.

Main results of the KAPRI include a literature study that covers the most essential content on the topic. A set of laboratory measurement data was collected and analyzed during the project. Digital waveguides were found out useful in the longitudinal stress wave modeling. The transversal stress waves can be modeled to some extent by using the FIR based approach. Preliminary steps in the acoustical analysis of the excavated tunnels were conducted.

Preface

This work was conducted during years 2012–2013. This work has been an extraordinary journey to the topic and in some scope it went even further than it was originally planned.

My gratitude goes to the Finnish Work Environment Fund for making possible this interesting research. I would like to thank everyone who has contributed to this project. Especially professor Vesa Välimäki for valuable advice and encouraging provided during the project. I would also like to give credit Dr. Julian Parker for his contribution. Finally I would like to thank my family for the support and understanding.

Vaasa, Thursday 19th December, 2013,

Sami Oksanen

Contents

Contents

6

Symbols and Abbreviations

Symbols

a	Area	[m^2]
c	Wave speed in fluid	[m/s]
d	Diameter	[m]
f	Frequency	[Hz]
$L(t)$	Longitudinal stress wave	[Pa]
$T(t)$	Transversal stress wave	[Pa]
Y	Young's modulus	[Pa]
ρ	Material density	[kg/m^3]
σ	Stress	

Abbreviations

APF	Allpass Filter
DWG	Digital Waveguide
FDTD	Finite Difference Time Domain
FIR	Finite Impulse Response
IIR	Infinite Impulse Response
SG	Strain Gage

List of Figures

1. Introduction

1.1 Motivation for the Study

Motivation for the study is two folded, first there is a need for a fast and computationally efficient test and development tool for drill steel noise generation investigation. Secondly, the sound generation mechanisms of the percussive drilling are not known. The objective of the study is to gain understanding on the drill steel sound generation.

Current drill steel modeling methods are computationally very expensive and therefore the analysis is restricted to a short time periods. There is a need to model drill steel vibrations for a series of impacts. The approach in this study is to model the drill steels using techniques that are used in musical instrument modeling.

1.2 Research Questions

Objective for KAPRI was to develop stress wave models to be more realistic. Secondary objective was to conduct laboratory measurements of audio signals generated by the steel vibrations. The objective was also to investigate environmental conditions that are presents at sites where rock drilling equipment is used.

1.3 Report Organization

This report is organized as follows. First a literature study of the relevant topics is presented in Section 2. The theory background of the drill steel vibrations is given in Section 3. Next, the sound and vibration anal-

ysis of steel bars under laboratory conditions is introduced in Section 4. Then, digital waveguide (DWG) modeling of the drill steel vibrations is explained in Section 5 and the model implementation from the software perspective in Section 6. Results for digital waveguide modeling of the stress waves in steel bars are presented and analyzed in Section 7. Then, acoustical analysis of excavated tunnels is presented in Section 8. Finally, summary and conclusions are given.

2. Literature Study

A literature study was conducted during the project where the most essential references were searched and their main contents were analyzed. The study was conducted using standard data search methods. Most of the material was available online, but some of the older articles were ordered as paper copies from the Aalto library. This study is limited to English references, but there is plenty of older material available written in other languages such as German. The main findings of the literature study are listed in the following subsections, which are roughly sorted based on the topic. Some of the references could have been sorted differently and therefore the reader is encouraged to go through all subsections for maximized coverage on the topics. The relevance of each reference within the scope of this project is evaluated using star notation after the individual references. If a reference was found to be very relevant to the project scope five stars ($\star\,\star\,\star\,\star\,\star$) were awarded. On the other hand, in case where a reference had not much in common with the project scope one star ($\star$) was awarded. Please note that this star rating has nothing to do with the quality evaluation of individual references.

2.1 Theory of Vibrations in Rods Related References

Wave motion in elastic solids (Graff, 1975) $\star\,\star\,\star\,\star$

The following text is taken from the book cover description: "This textbook presents comprehensive intermediate-level coverage of nearly all major topics of elastic wave propagation in solids. The subjects range from the elementary theory of waves and vibrations in strings to the three-dimensional theory of waves in thick plates."

The physics of musical instruments (Fletcher and Rossing, 1991)
⋆⋆

This textbook is oriented towards musical instrument acoustics. There is a section where vibration phenomena of rods are briefly explained.

Vibration – Fundamentals and Practice (De Silva, 1999) ⋆⋆⋆

This textbook is good starting point for vibration phenomena. It covers various topics in vibration and corresponding measurement techniques.

Modal testing: theory, practice, and application (Ewins, 2000)
⋆⋆⋆

This is a good textbook on modal testing. It focuses on various applications and measurement techniques involved in modal testing. It covers the theory, from experiment planning through to conducting actual measurements and to model construction based on the measured data.

Rigid impact - the mechanism of percussive rock drilling (Dongmin, 2008) ⋆⋆⋆

This paper gives a brief introduction to the mechanisms of the rock drilling. It is a compact presentation of the key elements of the process and offers a good starting point / tutorial of the topic.

2.2   Strain Wave Phenomena Related References

Investigation of noise and vibration in percussive drill rods (Hawkes and Burks, 1979) ⋆⋆⋆⋆⋆

The following text is taken from the article abstract: "This paper describes how longitudinal and bending stress waves in percussive drill rods generate noise. It is shown that in practical drills the largest noise source is the bending waves, which are mainly generated because of imperfections in the piston, chuck, and drill rod alignment. Equations are presented which enable the dominant frequencies of the noise spectra generated by the bending and longitudinal waves to be precisely predicted. Means for reducing the amplitude of the bending waves are discussed."

This paper gives an excellent starting point to the topics of the KAPRI

project.

Strain wave behavior in percussive drill steels during drilling operations
(Hawkes and Chakravarty, 1961) ⋆ ⋆ ⋆ ⋆ ⋆

The objective of this paper is to link measurements of operating drill steel to one-dimensional theory of longitudinal impacts of rods. This research focuses only on longitudinal stress waves. Pneumatic drilling equipment (Holman SL 200) with 8 and 10 feet long hexagonal rods with diameter of 3/8 in. were used in this study. Measurement setup consists of strain gauges and oscilloscope. The piston rod contact was monitored with a DC-voltage between piston and rod. The study shows that under special conditions (cylindrical piston without rotation) the energy between transversal and longitudinal waves are distributed in a 30% (transversal) to 70% (longitudinal) ratio. Three bit rock conditions are studied in this paper namely, normal rock contact, bit against steel plate and free end conditions.

Transmission of energy in percussive drilling – The influence of flexural strain waves in the drill steel (Roberts et al., 1962) ⋆ ⋆ ⋆ ⋆

The objective in this paper is to examine the transversal wave behavior in the drill steels. The introduction gives a brief look in to the basic rod vibration theory including equations for transversal wave speed estimation along to bar and shear velocities. The test apparatus used in the laboratory test includes vertical drop mass equipment. The drill steels used in the laboratory tests were cylindrical, whereas at the infield measurements hexagonal shaped bars were used. The rod had length of 120 in. and diameter of 0.742 in. The rod was spherically round shaped and one end had rounding which was set 0.25 in of the axis. Main results of this paper. Recorded transversal wave shapes along the rod. The dispersion effect is clearly visible. Transversal wave velocity was determined following manner. The disturbances are travelling at bar velocity 5200 m/s (17.060 ft/s). However, the main pulse speed was 2910–3140 m/s (9550–10300 ft/s). Transversal wave amplitudes had maximum values near the rod ends compared to values in the middle sections.

Experimental characterization of the noise generation mechanism of percussion drill rods (Lesage et al., 1997) ★ ★ ★ ★ ★

This paper describes a noise generation method for drill steel investigations in laboratory conditions. The described apparatus is capable of producing similar sound output than experienced in the field conditions in the laboratory. The major restriction of the apparatus is its capability to generate only single impacts. In realistic drilling conditions the drill steel is constantly vibrating whereas in this setup the drill steel is not vibrating at the time of impact. The difference between in situ and laboratory measurement can be seen from the plots. The impact stress generated by the apparatus is approximately 120 MPa compared to 290 MPa of actual drilling. The laboratory experiments show that 2 degree misalignment increases transversal wave generation at frequencies below 6 kHz up to 10 dBs.

The Generation of Bending Vibrations in Drill Rods (Carlvik, 1981) ★ ★ ★ ★

Following text is adapted from the article abstract. This paper presents a theoretical investigation of how much of the energy fed into the system can be expected to be converted to bending energy in the drill rod. The model considered is simple, an integral drill steel with the rock response represented by an eccentrically acting viscous damper, but it is believed to give qualitively correct answers.

The results indicate that in a typical situation, one can expect about 10% of the incident stress wave energy to be converted to bending. For a system with a detachable drill bit the fraction is probably less. The form of the incident stress wave is not important, although a steep front tends to give more bending. A heavier piston reduces the bending fraction.

Strain waves in colliding bars having nonparallel faces (Erem'yants and Slepnev, 2006) ★ ★ ★

This paper presents an experimental investigation on the amount of bending stress generation caused by an impact of nonparallel surfaces. Based on the presented results the bending stress levels are increasing most rapidly when the miss alignment angle varies from 0 to 0.5 degrees. After that the increase of bending waves is much slower. As an example of having piston impacting at velocity of 5 m/s the resulted longitudinal

strain level with perfectly aligned impact is approximately 100 MPa and with 0.5 degree misalignment the bending stress level is approximately 80 MPa. For misalignment of 1.5 degrees the bending stress is approximately 110 MPa and longitudinal stress is approximately 80 MPa.

The determination of stress waveforms produced by percussive drill pistons of various geometrical designs (Dutta, 1968) ⋆ ⋆ ⋆ ⋆ ⋆

This paper investigates stress waveforms being produced by different piston shapes. This paper presents a waveguide approach to stress wave behavior in the rod and piston. A computer program (Mercury Autocode) for computing the stress wave shapes is presented in the Appendix.

Analysis of elastic flexural waves in non-uniform beams based on measurement of strains and accelerations (Hillström and Lundberg, 2001) ⋆⋆

The aim of the paper is to introduce a method for evaluating of the time histories of shear force, transverse velocity, bending moment and angular velocity at desired section based on measurements in four quantities or four different locations. The model is developed based on Timoshenko beam model. The method is validated using measurements of an aluminum beam.

Identification of a percussive drill rod joint from its response to stress wave loading (Berzi et al., 1996) ⋆

This paper investigates rod joint identification based on its response to stress wave loading. The paper presents a method where nonlinear dissipative spring mass model parameters are set based on the actual measurements. It is still out of the scope of the POKA and KAPRI projects.

Elastic bar transfer function determination using two-point strain measurements (Kaczmarek, 2009) ⋆ ⋆ ⋆ ⋆

A transfer function of an elastic bar is determined based on measured strain at two points along the bar. The transfer function is determined with a deconvolution method in frequency-domain. The assumption for the transfer function estimation is that the forward going and backwards propagating waves are not overlapping during the measurement. The modeled transfer function is then used to estimate strain in a virtual po-

sition. The method seems to produce reasonable results for a short estimation period ($\approx 110\ \mu$s) for a bar length of 2.5 m.

Passbands for acoustic transmission in an idealized drills string (Barnes and Kirkwood, 1972) $\star\star$

This paper presents a theoretical approach to finding the optimal channels for acoustic transmission along a drill string from DTH bit to the top of the string. The acoustic transmission is based on longitudinal waves. Feasible bands for transmission were found around 3 kHz where lowest torsional modes do not cause interference to the transmission.

Sound transmission through a periodic cascade with application to drill pipes (Lous et al., 1998) $\star\star$

The following description is taken form the paper abstract. The approach discussed in this paper has the advantage that it yields explicit expressions for the fine structure of the drill pipe's frequency response in the pass bands. It furthermore allows the effect of energy dissipation and pipe segment length variations to be included in the model. The emphasis of the paper, however, lies on the time domain modeling of the drill pipe. The propagation of sound energy pulses through its wall, and the effect of multiple reflections and/or transmissions during this propagation, are described using a Markov chain. Explicit expressions result for the expected duration of an energy pulse's trip from one end of the drill pipe to the other, depending upon the number of drill pipe segments and the transmission coefficient at the tool-joints connecting them. The results are applicable to any situation where sound or energy transmission through a cascade of acoustic components occurs.

Wave impedances of drill strings and other periodic media (Drumheller, 2002) $\star\star\star$

This paper is an extension to sound transmission in periodic cascade. The modeled approach utilizes eigenvectors in transmission impedance determination. There is an interesting section in the paper Appendixes that describes the wave amplifier and wave separation.

Assessment of hand-type hammer drill bits under percussive loading (Demir, 2007) ⋆ ⋆ ⋆ ⋆

This Master's thesis offers a good literature survey on the stress waves of percussive drilling. Thesis provides also a FEM approach to stress wave modeling. The Appendix offers a nice review to impact mechanics.

2.3 Drilling Noise Reduction Related References

Transient acoustic radiation from impacted beam-like structures (Akay et al., 1983) ⋆ ⋆ ⋆ ⋆ ⋆

This paper describes a method to estimate a sound field in a given point that is radiated from an impacted beam. The presented method is based on the finite element model of the beam. The sound radiation is modeled using an array of dipole sources placed on a suitable distance from each other. The required amount of the dipole sources is also discussed in the paper. The paper presents radiation patterns for different modes. This is a good starting point for attempts to connect modeled stress waves and related sound output.

A review of impact noise (Akay, 1978) ⋆ ⋆ ⋆ ⋆

This paper is a good starting point for studies in the field of impact noise. Following text is taken from the paper abstract. In this paper, available literature concerned with impact noise generation and control is reviewed with emphasis on generation mechanisms. Basic research studies are considered under five different classes according to the mechanism of sound generation. These are air ejection, rigid body radiation, radiation due to rapid surface deformations, pseudo-steady-state radiation, and sound radiation due to material fracture. A brief characterization of impact sounds in addition to a description of efforts to standardize impact noise exposure criteria is given in the Introduction. A bibliography on impact noise control is included in order to permit assessment of the state of the art.

Measurement and analysis of the stress wave generated rod noise in percussive rock drill (Dutta et al., 1981) ⋆ ⋆ ⋆

This paper introduces a set of measurements of stress wave generated noise. The measurements are divided into three different approaches namely, manual impact, pendulum impact and real drill impact. Results in this paper are similar to ones presented in Hawkes and Burks (1979). This paper is probably a short version submitted to a conference. It seems that all the necessary information on the paper topic is already covered in more detailed manner in Hawkes and Burks (1979).

Iskuporauksen kankimelusta (Tanttari and Saarinen, 1995) ⋆⋆

This paper gives a brief introduction to the sound generation of the drill steels. It also presents a method to estimate sound radiation mechanism of the drill steels. The method is based on two microphones placed on the opposite sides of the drill steel. Then the phase of cross correlation between audio channels is investigated. Longitudinal modes can be found at frequencies where absolute value of the phase is close to zero degrees, transversal modes can be found at frequencies where the absolute value of the phase is close to 180 degrees. This method was found to be useful only in laboratory conditions with single impacts.

Concentric drill steels for noise reduction of percussion drilling (Stein and Aljoe, 1986) ⋆

A concentric drill steel design is presented in this paper. The main idea is to use two layered drill steel in order to minimize the transversal vibrations. The inner core is used to transmit the longitudinal pulses to the rock and the outer core is used to transmit required tongue for drill bit rotation. The inner and the outer cores are acoustically isolated with elastomer isolators distributed along the rod. Using such design the overall noise level can be decreased by 5 dBA. And the drill steel noise level by 8 dBA.

2.4 Strain Wave Modeling Related References

Microcomputer simulation of percussive drilling (Lundberg, 1985) ⋆ ⋆ ⋆ ⋆ ⋆

This paper presents a computer program for modeling churn drilling, DTH drilling and hammer drilling. The computational approach is based on the previously published papers for modeling non uniform drill steel Lundberg (1981)[1] and for bit rock model Lundberg (1982). The implementation of the computational model presented in this paper is not described in a detailed manner.

Analysis of Piano Tones Using an Inharmonic Inverse Comb Filter
(Lehtonen, 2008) ⋆ ⋆ ⋆ ⋆ ⋆

This paper presents analysis methods for inharmonic piano sound analysis. A FIR filter based approach was found more accurate in the dispersion filter design compared to a cascade of second-order allpass filters. The FIR dispersion filter design procedure is used also in the DWG model for transversal vibration in drill steels, presented later in this report. The inverse comb filter procedure is used for picking partials from recorded piano tones. Perhaps this could also be used in some form in the drill steel strain wave analysis.

Splitting the Unit Delay (Laakso et al., 1996) ⋆ ⋆ ⋆ ⋆ ⋆

This paper covers the fractional delay scheme. It presents several design concepts for FIR and allpass filters. This paper has also many practical examples of the fractional delay filter use cases.

Physical Modeling using Digital Waveguides (Smith, 1992) ⋆ ⋆ ⋆ ⋆ ⋆

This paper gives a good introduction using digital waveguides (DWGs) in physical modeling. The paper starts with an example of vibrating ideal string. The paper explains the usage other type of waves that can be used in DWG modeling, such as power and energy density waves. Frequency dependent losses are also presented. Paper has also a c-code example for

---

[1]B. Lundberg, Microcomputer simulation of longitudinal impact between nonuniform elastic rods. IJMEE **9**, 301–315 (1981). By the time of writing this the original paper was not available.

plucked string.

Numerical Sound Synthesis: Finite Difference Schemes and Simulation in Musical Acoustics (Bilbao, 2009) ★★★★★

This book is an excellent tutorial on solving partial differential equations in vibration problems via finite difference techniques, for the purpose of sound synthesis. The focus is musical acoustics, and most of the structures considered have their main application in that area. However, many are general enough to apply to other problems. Of particular interest with respect to drill-steel vibration are the sections on bar and string vibration, which cover many interesting cases including stiff-strings, non-uniform bars and non-linear string vibration.

Robust, Efficient Design of Allpass Filters for Dispersive String Sound Synthesis (Abel et al., 2010) ★★★★

This paper describes a computationally effective method for dispersion filter design. The implementation is based on a cascade of second-order allpass filter sections. This method could be worth of trying to achieve increased accuracy at the lower frequencies in the future KAPRI project.

3. Vibrations in Drill Steels – Theoretical Approach

3.1 Stress and Strain Relation

The following introduction to the stress strain relation is adopted from (Kyowa Electronics Instruments CO., LTD., 2011). The stress σ is defined by the relation between external force P and cross-sectional area A of the object under investigation

$$\sigma = \frac{P}{A} \quad \text{[Pa]}. \tag{3.1}$$

The strain ϵ caused by stress σ is dependent on the material parameter E known as Young's modulus

$$\epsilon = \frac{\sigma}{E}. \tag{3.2}$$

A typical value of Young's modulus for material used in drill steels is approximately 220 GPa. Polarity of the strain determines the nature of the strain wave. Strain receives positive values when object of interest is exposed to tensile strain and negative strain values indicate compressive strain.

3.2 Longitudinal Stress Waves

The longitudinal stress waves are generated by Poisson's ratio expansions and contractions of the rod as the longitudinal waves travel back and forth in the steel bar. The longitudinal waves are responsible for transmitting the energy along the steel to bit and further to the rock Hawkes and Burks (1979).

3.3   Transversal Stress Waves

Transversal stress waves are a byproduct of percussive drilling. Transversal vibrations are generated by misaligned impacts, interaction in the bit-rock interface and worn drilling equipment. The transversal vibrations contribute the majority of the sound output compared to the longitudinal stress waves Hawkes and Burks (1979).

3.4   Wave Speed and Modal Frequencies for Drill Steels

The following formulation follows the presentation in Hawkes and Burks (1979). The longitudinal wave speed C_{L} in a material is determined by the material dependent parameters of Young's modulus E and density ρ

$$C_{\mathrm{L}} = \sqrt{E/\rho}. \tag{3.3}$$

The frequency dependent transversal wave speed C_{T} can be formulated

$$C_{\mathrm{T}} = \sqrt{(\pi/2)(df_b C_{\mathrm{L}})}, \tag{3.4}$$

where d is the drill steel diameter, f_b is the transversal wave frequency.

The modal frequencies for a drill steel with length of L_{r} for longitudinal modes is given by

$$f_{Ln} = \frac{nC_L}{2L_r}, \tag{3.5}$$

where n is the mode index. Natural frequencies of the transversal vibrations in a drill steel can be found for frequencies where the drill steel length L_r is a half of the wavelength. The drill steel modal frequencies can be determined based on the physical dimensions and for the transversal modes by

$$f_{Bn} = \frac{n^2 \pi d C_L}{8 L_r^2} \left[1 - 1.2 \left(\frac{nd}{L_r} \right)^2 \right] \left(\frac{2n+1}{2n} \right)^2, \tag{3.6}$$

where n is the mode index. Middle correction term (inside square brackets) is the correction term to take into account the rotary inertia and the shear force using the Timoshenko beam theory. The Timoshenko correction factor should be applied when $nD/L_r < 0.4$ .The last term of the Equation is the drill steel end condition correction factor for free-free (F–F) end conditions (see Table 1 from Hawkes and Burks (1979) for corresponding values for different end conditions).
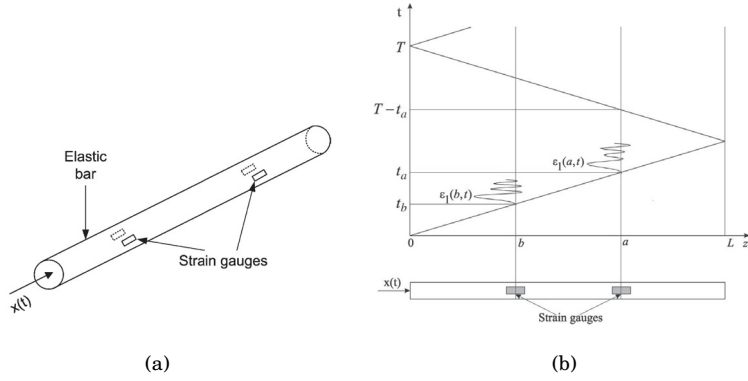
Figure 3.1. Measurement setup for the drill steel transfer function estimation after Kacz-
marek (2009). (a) Strain gauge placement, (b) Lagrangian diagram for longi-
tudinal waves in cylindrical bar.

3.5   Drill Steel Transfer Function for Stress Waves

Following method is described in a more detailed manner in Kaczmarek
(2009). Estimation of a stress wave transfer function in a drill steel can
be utilized in stress wave signal post processing. The estimated transfer
function is empirically derived using simultaneous stress wave measure-
ments at two points along the drill steel. Measurement points need to
be placed in such way that stress wave are separated by propagation di-
rection at the measurement points. The estimated transfer function is
constructed based on a deconvolution in frequency domain. The measure-
ment setup is presented in Figure 3.1.

3.6   Transmission and Reflection of Stress Waves at Drill Steel Joints

When travelling stress wave meets a sudden change in cross section of the
drill steel part of the initial stress wave is reflected back from the bound-
ary and the reminder of the stress wave will be transmitted along the
steel. Following definition of the stress wave transmission and reflection
at cross-section boundaries is based on Dutta (1968).

The transmission coefficient T_c and reflection coefficient R_c are deter-
mined based on the rod diameter d_1 before and after d_2 the boundary

$$T_c = \frac{2d_2^2}{d_1^2 + d_2^2}, \qquad R_c = \frac{d_2^2 - d_1^2}{d_1^2 + d_2^2}. \tag{3.7}$$

For more detailed derivation of the reflection and transmission coefficients
see Dutta (1968).

3.7   Drill Steel Boundary Conditions

The boundary condition inspection is divided into two approaches. First a linear boundary condition based on a constant reflection coefficient at the boundary (Hawkes and Burks, 1979). Secondly a nonlinear approximation on the stress wave behavior at the bit rock interface based on the drill bit movement equations (Li et al., 2001; Lundberg, 1982). Both boundary condition classes are discussed in following Sub-Sections.

3.7.1   Theoretical Boundary Conditions

A simple way to define boundary conditions for the drill steel is to let it vibrate freely without any restrictions at the boundaries. This will lead to stress waves to reflect from the boundaries having opposite sign. However this boundary condition is only valid situations where the steel is rigged using nylon threads i.e. under laboratory conditions. More realistic approach is to use a boundary condition where the drill steel is attached to a rigid surface or object. In an ideal case this clamped boundary condition will produce full reflection of the incoming stress wave (Graff, 1975).

4. Sound and Vibration Analysis in Laboratory Conditions

4.1 Measurement Domains and Equipment

4.1.1 Acoustical Measurements

Acoustical measurements were carried out during the strain wave measurements. The microphones were placed in the proximity of the exited objects (See Fig. 4.3. Measurement equipment consisted of B&K 4191 microphones, B&K 2669 pre-amplifiers and B&K Nexus 2690 microphone condition amplifier. The audio measurement equipment was connected to the RME FireFace 400 audio interface.

4.1.2 Strain and Stress Wave Measurements

A strain gage is a resistive component which is tightly attached to the surface of the object under investigation. When the object is exposed to compressive or tensile loading the strain gage resistance will change slightly based on the gage length variation. The change in resistance can then be monitored with a Wheatstone bridge circuit (see Fig. 4.1(a)) and signal conditioning amplifier.

Strain gages can be utilized in various Wheatstone bridge topologies. When two strain gages are attached to the bridge a half-bridge topology is formed, see Figures 4.1(d) and 4.1(c). This can be used to measure longitudinal or transversal strain waves at desired point if the strain gages are placed on the opposite sides of the object. The half-bridge topology requires only a single channel signal condition amplifier.

One active strain gage topology (quarter-bridge) can be used to determine strain in single point measurement(see Fig. 4.1(b)). If two strain

gages are placed on the opposite sides of the object both longitudinal and transversal strain waves can be measured at once. However, this requires a two-channel signal conditioning amplifier.

Half-Bridge Topology

Half-bridge topology is used when either longitudinal (see Fig. 4.1(c)) or transversal (see Fig. 4.1(d)) strain waves are measured. The strain gages are attached on the opposite sides of the object under investigation. The Wheatstone bridge is connected according to the desired measurement outcome.

Quarter-Bridge Topology

The measurement circuit is initialized so that the bridge is balanced and output voltage e is 0V. When stress is applied and the length of the strain gage changes the bridge output voltage is determined by following equation:

$$e = \frac{1}{4}K\epsilon E, \qquad (4.1)$$

where K is the gage factor, ϵ is the stress and E is the bridge supply voltage. The gage factor is dependent on the gage construction and is given by the gage manufacturer. When using quarter-bridge topology with two signal channels, the longitudinal and transversal strain waves can be determined simultaneously. The bridge output voltage is determined by the following equations:

$$e_{\mathrm{T}} = \frac{1}{4}K(\epsilon_1 - \epsilon_2)E, \qquad e_{\mathrm{L}} = \frac{1}{4}K(\epsilon_1 + \epsilon_2)E, \qquad (4.2)$$

where e_{T} is the is the transversal strain wave output, and e_{L} is the longitudinal strain wave output.

Strain Wave Signal Conditioning Amplifier

A custom amplifier (AALTO) was designed and built for the strain wave measurements. The core of the amplifier is a Texas Instruments INA 111 precision measurement amplifier circuit. The amplifier has four parallel channels and each supports quarter- and half-bridge topologies. A schematic of one amplifier channel is presented in Figure 4.2.

The amplifier was designed for 120 Ω bridge impedance. The strain gages used in the measurements were manufactured by KYOWA. The strain gages matched for steels thermal expansion coefficient (KFG-5-

(a)

(b)

(c)

(d)
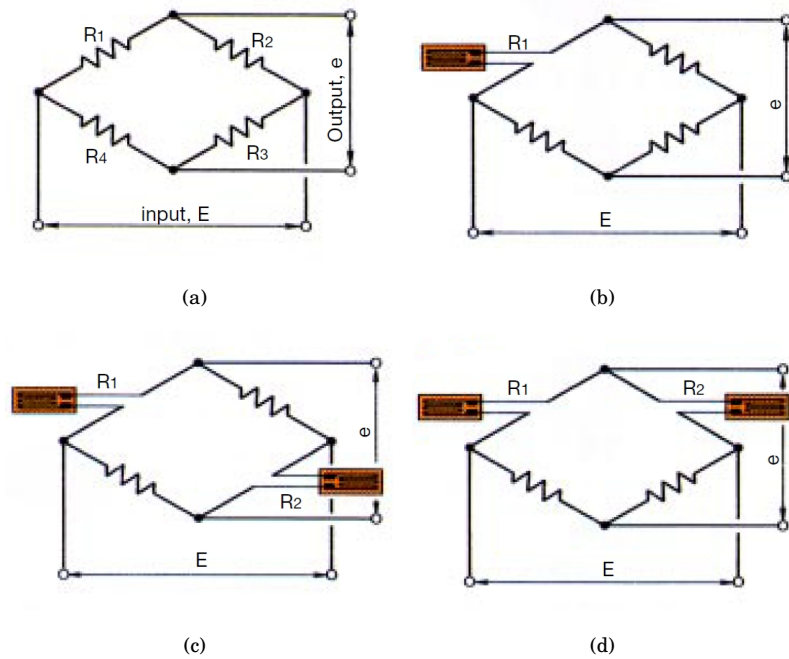
Figure 4.1. Strain gage measurement topologies (a) Wheatstone bridge circuit with four resistors (b) Quarter-bridge topology with one strain gage (c) Half-bridge topology for longitudinal strain wave measurement (d) Half-bridge topology for transversal strain wave measurement (All figures are adopted from Kyowa Electronics Instruments CO., LTD. (2011)).

120-C1-11L1M2R) had a nominal resistance of $119.6 \pm 0.4\ \Omega$ with active length of 5 mm and gage factor of 2.08 ± 1.0 %.

4.1.3 Laser Vibrometer Measurements

Drill steel surface vibration was measured at some instances using a Doppler laser vibrometer (Polytecnic OFV-3001). The laser beam was focused on the proximity of the strain gages to be able to compare the results from the strain gages and surface velocity measurements.

4.2 Measurement Procedure and Arrangements

4.2.1 Measurement Procedure

Measurements were conducted at the Aalto University Department of Signal Processing and Acoustics. The large anechoic chamber was used
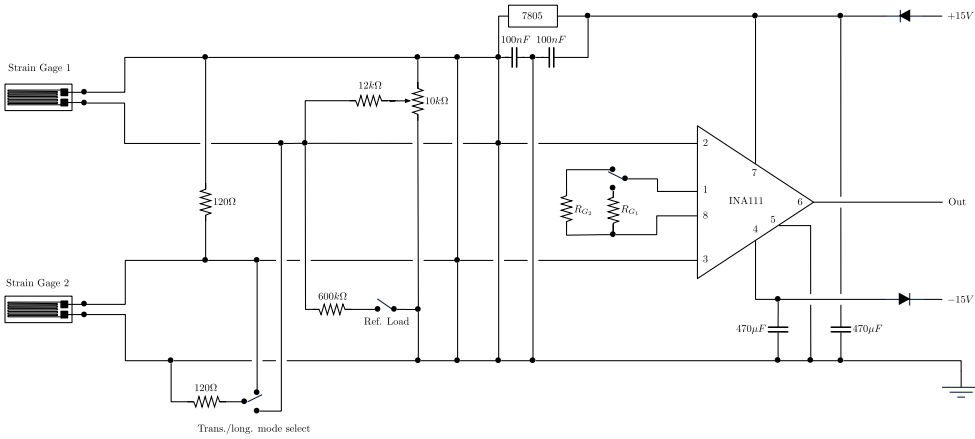
Figure 4.2. Signal condition amplifier schematics for one channel. The layout is designed for half-bridge topology, in case a quarter bridge topology is required the Strain Gage 2 can be replaced with a 120 Ω resistor.

during the measurements. The overall view of the measurement arrangements is presented in Figure 4.3 where a drill steel is being measured. The drill steel is attached to a custom-made holder (Figures 4.4(a) and 4.4(b)) which consists of aluminium tubes filled with insulation foam to damp the structure vibrations. The drill steel holder is attached to the permanently installed vertical poles inside the anechoic chamber. The drill steel is mounted on the holder at two points using thread and neoprene dampers. Neoprene dampers are used to isolate vibration transmission between the drill steel and holder.

The drill steel was excited by hitting it to the impact end using a hand-held cylindrical impact device (Figures 4.4(c) and 4.4(d)). Using a cylindrical shaped object instead of forge hammer produces more realistic strain wave pulse shapes. However, the excitation signal is only repeatable to a limited extent. More reliable results could be achieved using a device which could produce more repeatable impacts.

Current setup limits parallel strain measurements to two channels. It is possible to measure strains at two different points using the Wheatstone bridge in half-bridge mode. However, using the half-bridge mode requires pre-selection of the observed wave polarity (longitudinal or transversal). Based on this limitation the measurements were conducted as a series of two channel measurements.

The measurement setup consisted of the following main components

1. Custom-made strain wave signal conditioning amplifier for the strain wave measurements (see Sec 4.1.2)
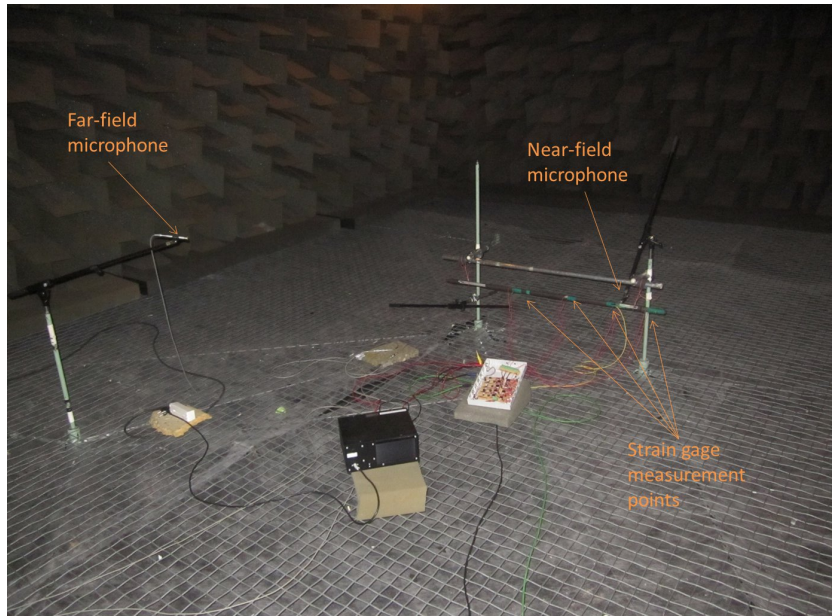
Figure 4.3. Overall view of the measurement setup placed inside the anechoic chamber. The drill steel under investigation is rigged to the mounting frame. The audio signals are captured using near- and far-field microphones. Strain waves are captured using a set of strain gage measurement points. The custom-made strain wave signal conditioning amplifier and its power supply are in the middle of the figure.

2. Audio measurement equipment (see Sec. 4.1.1).

3. RME FireFace 400 audio interface and a laptop PC for the measurement data collection. Frequency response characteristics taken from the data sheet (http://www.rme-audio.de/en_products_fireface_400.php):

- Frequency response AD/DA, -0.1 dB: 5 Hz - 20.4 kHz (fs 44.1 kHz)

- Frequency response AD/DA, -0.5 dB: 1 Hz - 43.3 kHz (fs 96 kHz)

- Frequency response AD/DA, -1 dB: 1 Hz - 80 kHz (fs 192 kHz)

Note, the data sheet is included in the final deliverable.

4.2.2 System Calibration

The measurement system was calibrated for the future reference. The acoustic signals were calibrated using B&K 4231 microphone calibrator.

(a)   (b)

(c)   (d)

(e)
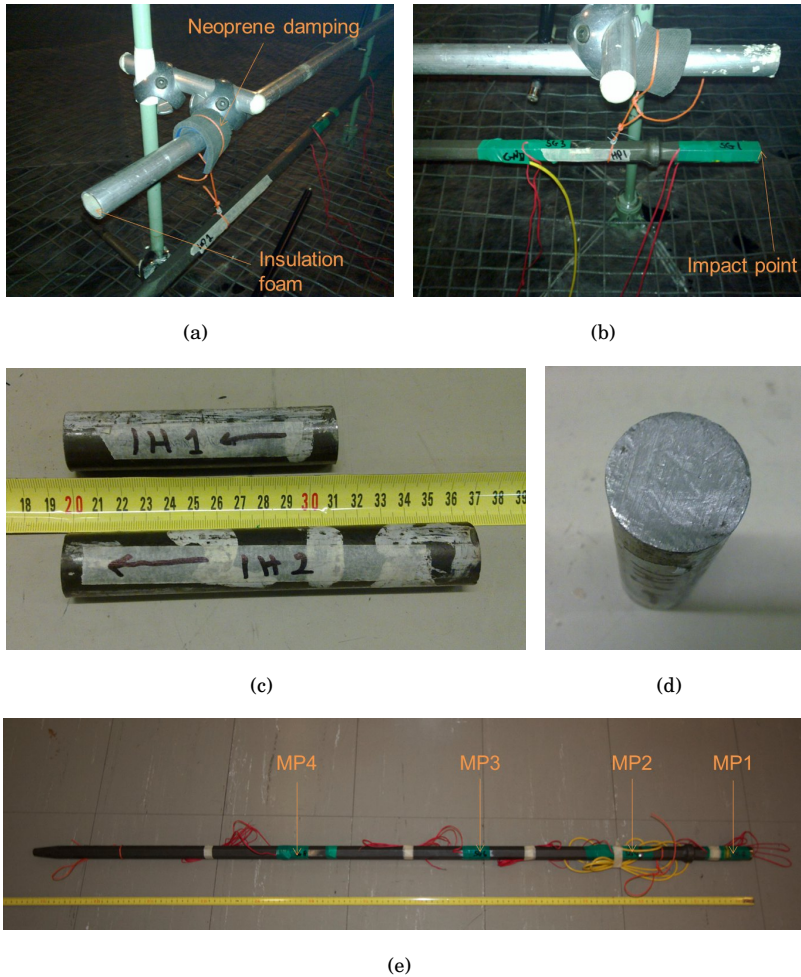
Figure 4.4. Measurement arrangements: Drill steel rigging to the support frame (a and b), impact devices (c and d), and instrumented integral drill steel (e).

The reference level is 1 Pa / 94 dB SPL. The calibration signals were recorded in the beginning and in the end of measurements. The strain wave signals were calibrated by measuring the exact bridge feed-voltage. The absolute voltage level at the audio interface was calibrated using a signal generator feeding 50 mV PP test signal. The test signal is a mix of sinusoidal square and triangular waves at 1 kHz and 10 kHz frequencies. Bridge supply voltages are presented in a separate measurement log.
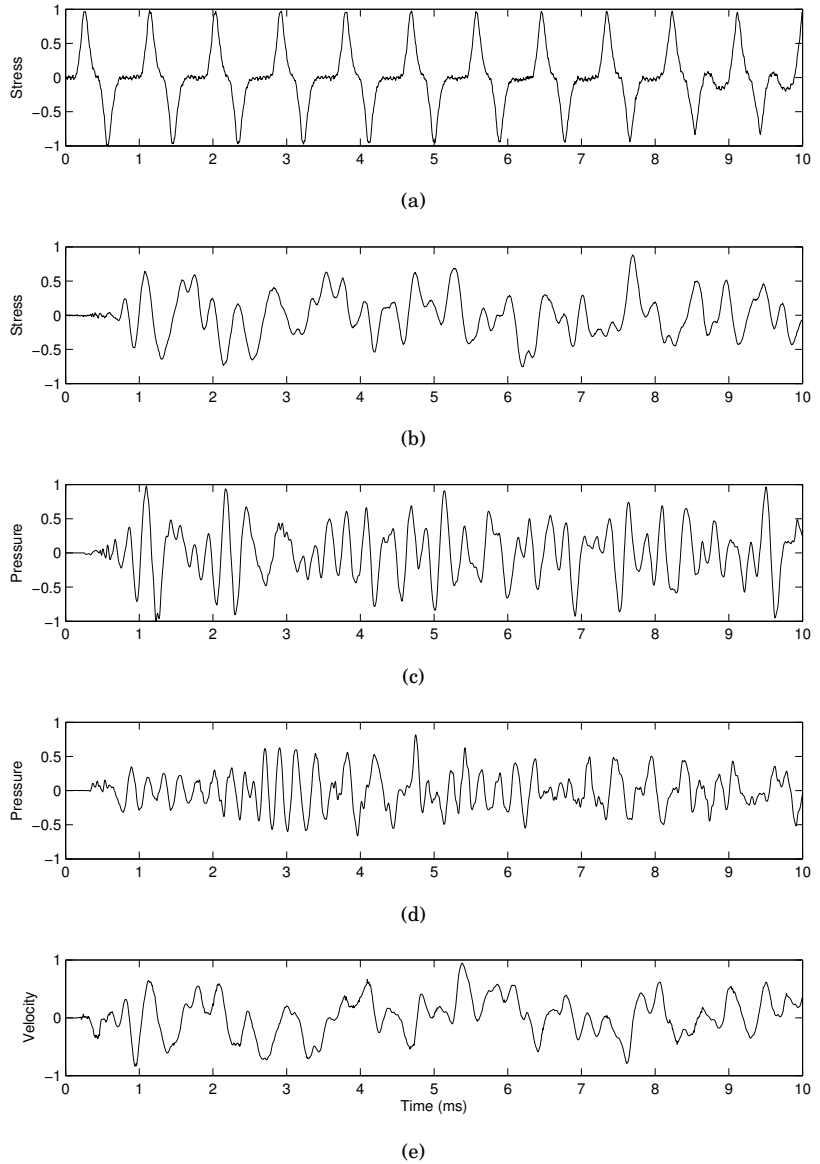
Figure 4.5. Measured signals in time-domain: (a) longitudinal stress waves (b) transversal stress waves, (c) near-field audio signal (d) far-field audio signal, and (e) surface vibration speed from laser vibrometer. Note, signals are individually scaled to range from -1 to 1.
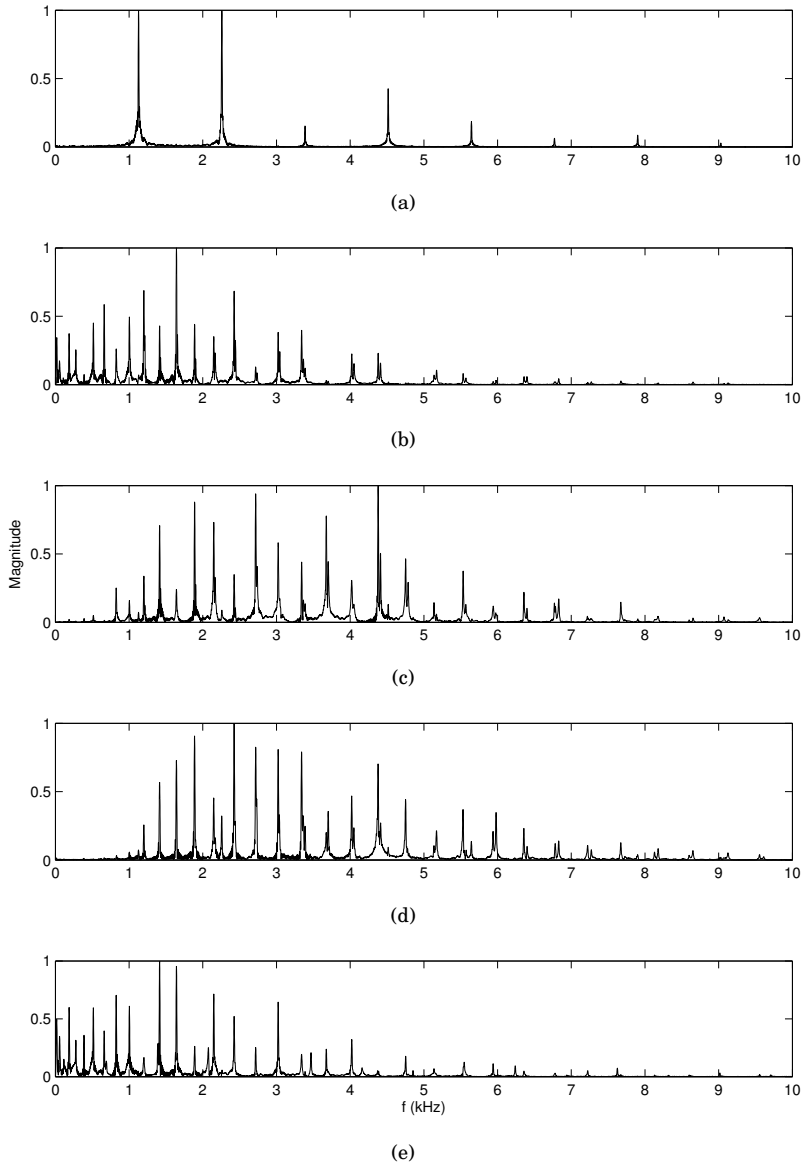
Figure 4.6. Measured signals in frequency-domain: (a) longitudinal stress waves (b) transversal stress waves, (c) near-field audio signal (d) far-field audio signal, and (e) surface vibration speed from laser vibrometer.

4.3 Drill Steel Dispersion Measurement

The dispersion measurements were conducted in the large anechoic chamber. The measurement setup is based on the previous setup, although some modifications to the drill steel holder and impact device were made during the measurements. Note, signals are individually scaled to range from 0 to 1.

4.3.1 Measurement Equipment

The measurement setup is presented in Figure 4.3. The drill steel[1] (Figure 4.4(e)) is attached to a custom-made holder. There were total of four measurement points and in each point a set of transversal and longitudinal stress waves were measured. Measurement point 1 (SG1 and SG2) was the reference point in all measurements. The strain waves were recorded for 10 individual impacts in each measurement point for transversal and longitudinal waves. After each impact the drill steel was damped placing fingers around it to ensure that drill steel was not vibrating and that the initial conditions were identical in each impact.

The strain gages (KFG-5-120-C1-11L1M2R, cage factor $2.081.0\%$, $R = 109.60.4$) were mounted in pairs along the drill steel. Each pair of gages was installed on the opposite sides of the drill steel. The strain gage installation followed the manufacturer procedure from the surface preparation to the gluing. The installation was finalized by adding a protective layer of tape on top of the strain gages and lead wires.

The strain gage signals were amplified using the AALTO amplifier (channels 2 and 4) and RME FireFace 400 audio interface (Analog 1 and 2). To provide sufficient signal levels, the strain gage signal from the AALTO amplifier was then amplified using +20dB gain in the audio interface.

The acoustic signals were recorded simultaneously along the strain waves. The acoustical measurement system consisted on two microphones (Fig. 1), one positioned next to the drill steel (Near-field) and another at approximately 2.5 m distance (Far-field). The microphones (B&K 4191, free-field) were connected to B&K 2669 pre-amplifiers which were connected to B&K Nexus signal conditioning amplifier. The Nexus outputs were then connected to the audio inter-face (channels 5 and 6).

---

[1]Hexagonal, 7870-6112-11, l=1220mm, d=22mm, 12 DEG, 110623
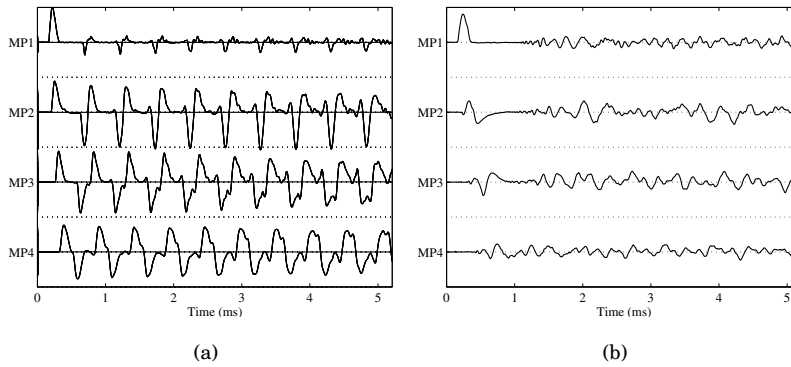
Figure 4.7. Time-domain inspection of measured strain waves, both longitudinal (a) and transversal (b). Strain waves are presented for each measurement point (MP1–MP4). Due to system limitations each strain wave is recorded from an individual excitation so the responses are not directly comparable to each other. Signals are not scaled to any physical quantity.

4.3.2 Time-domain Inspection

Measured signals were analyzed in time domain to verify the signal quality. Time-domain plots of longitudinal and transversal strain waves in each measurement point are presented in Figure 4.7. The shape of longitudinal wave near the impact point (MP1) is dominated by the initial impact, compared to the other measurement points (MP2-MP4). The initial impact is also visible in the transversal wave plots in measurement points MP1 and MP2. The dispersion effect is clearly visible in the strain waves from measurement points MP3 and MP4. The "chirp" caused by dispersion can be distinguished from the MP1 signal. Please note that signals are not scaled to match any physical quantity.

4.3.3 Spectral Inspection

Spectral analysis of strain waves was conducted in Matlab using `envel` and `findpeaks` functions for spectral peak estimation. The spectral peaks for measured transversal strain waves of 10 different impacts are presented in Figure 4.8. The detected spectral peaks are marked with red dots and computational peak locations with dashed lines. The computational peak locations are determined by Eq. 3.6 using rod prop function.

Please note, the computational modal frequencies matches the measured peaks when using the drill steel diameter of 19.5 mm (this value
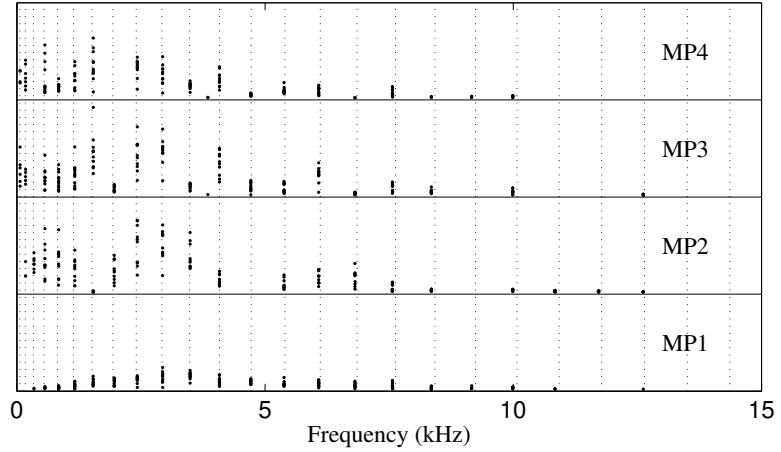
Figure 4.8. Measured transversal modes for ten different impacts for all measurement points. Estimated transversal modal locations are plotted with dashed lines.
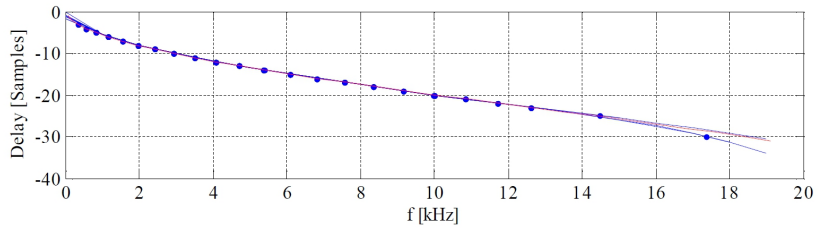
Figure 4.9. Dispersion curve fitting. Measured spectral peaks for 10 impacts are marked with blue dots, estimated phase delay curves for individual measurements with blue lines. The reference curve is plotted with red line.

was found iteratively) instead of 22 mm of the hexagonal drill steel true diameter. By the time of writing this report it is not clear what is causing this feature. One explanation can be the assumption of a round rod for transversal wave speed computation.

4.3.4 Dispersion Curve Fitting

The reference dispersion curve was determined based on the computed transversal modal frequencies. Then the dispersion curve is derived based on the assumption that phase is a multiple of 2π radians at every modal frequency.

The measured dispersion curves are constructed based on the measured spectral peaks. The phase curve for modal frequency $f_B n$ is determined by $\theta(\omega) = -2n\pi$. The closest matching index n is approximated by finding the nearest value of n from the reference frequencies. The reference and measured phase curves (MP1) are presented in Figure 4.9.

4.4 Cascade of Drill Steels

The effect of increasing the length of a drill steel by cascading the steels was examined in the laboratory conditions. A set of measurements were conducted with hexagonal drill steels having M-M threads with separate coupling sleeves. The drill steels were instrumented with a pair of strain gauges placed in the proximity of the drill steel center point. The cascade of three drill steels was rigged to the measurement system and the threads were tightened by using two monkey wrenches to approximately similar level. A series of impacts was applied to the end of the cascade using the hand-held impact device. The threads were getting looser at every impact because there were no rotation in the cascade to keep the threads tight. An example of the time domain response and frequency spectrum for longitudinal stress waves is presented on Figure 4.10 and for transversal stress waves in Figure 4.11.

4.4.1 Longitudinal Stress Waves

When the thread couplings are tight the longitudinal stress waves are effectively transmitted through the cascade (Figures 4.10(a) and 4.10(b)). Once the coupling starts to loosen up the stress wave shape starts to change (Figures 4.10(c) and 4.10(d)). When the couplings are extremely loose the initial stress wave is transmitted to the end of cascade (Figures 4.10(e) and 4.10(f)). The spectral plots show the change in longitudinal resonance frequencies as the effective cascade length is changed.

4.4.2 Transversal Stress Waves

The amount of generated transversal vibrations is increasing as the threads are loosening up. The spectral investigation reveals that majority of the transversal vibrations are concentrated to frequencies below 5 kHz when the couplings are tight (Figures 4.11(a) and 4.11(b)). Once the threads are getting looser the energy of the transversal modal frequencies is packed to the lower modes (Figures 4.11(c) and 4.11(d)). There is a significant change in the modal distribution of the transversal vibrations when threads are extremely loose (Figures 4.11(e) and 4.11(f)).

Figure 4.10. Measured **longitudinal** stress waves in drill steel cascade with variable coupling sleeve tightening levels. Time-domain in top subplot and frequency-domain in bottom subplot. (a) First steel tight coupling, (b) last steel tight coupling. (c) First steel medium coupling, (d) Last steel medium coupling. (e) First steel loose coupling, (e) last steel loose coupling.
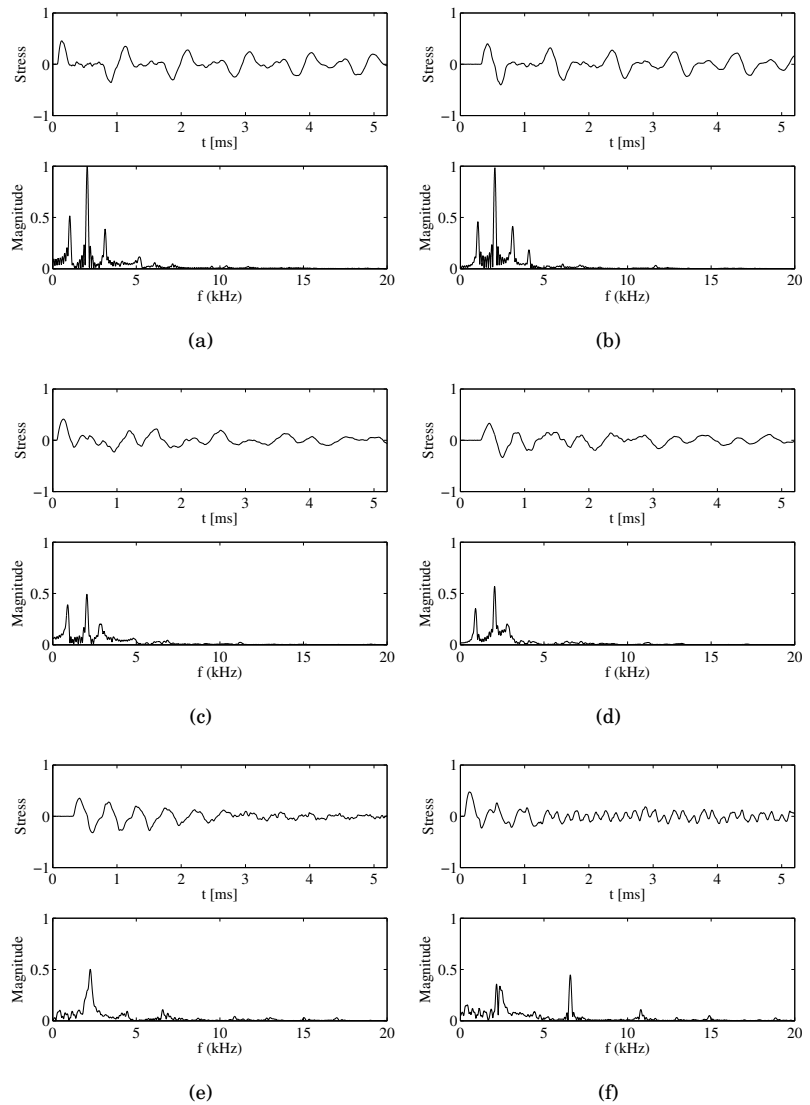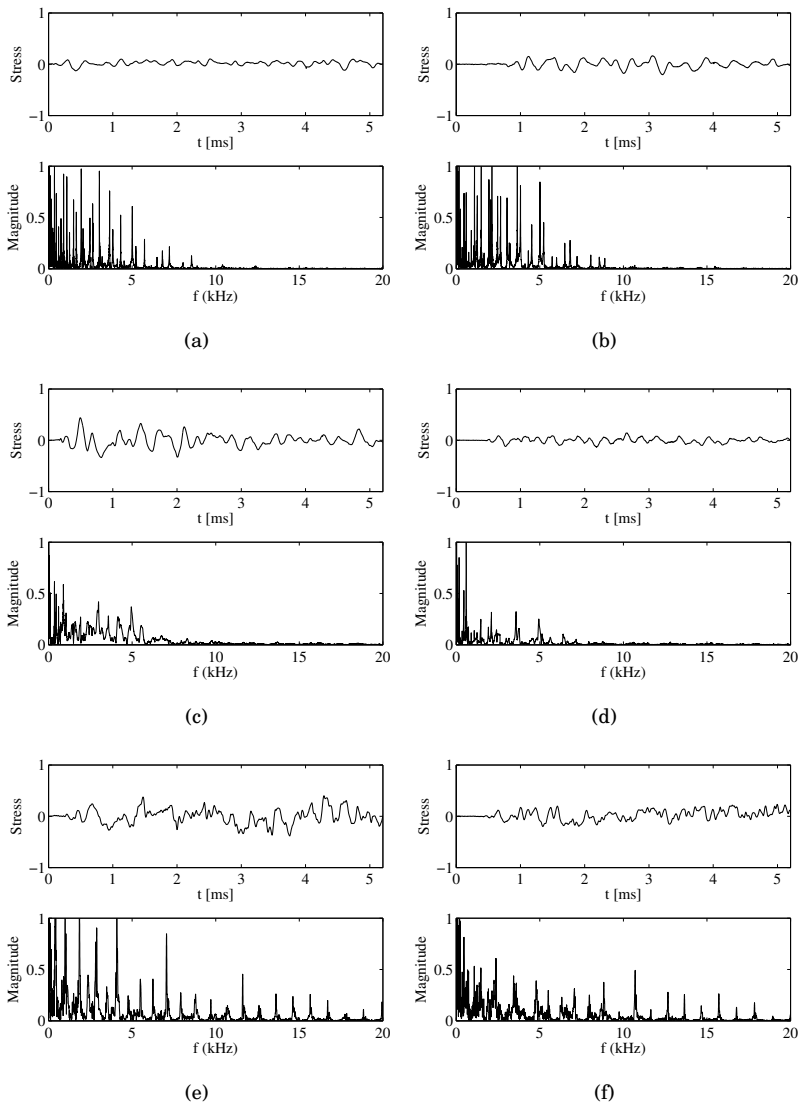
Figure 4.11. Measured **transversal** stress waves in drill steel cascade with variable coupling sleeve tightening levels. Time-domain in top subplot and frequency-domain in bottom subplot. (a) First steel tight coupling, (b) last steel tight coupling. (c) First steel medium coupling, (d) Last steel medium coupling. (e) First steel loose coupling, (e) last steel loose coupling.

5. Digital Waveguide Modeling of Strain Waves in Steel Bars

5.1 Longitudinal Stress Wave Model

Introduction to KAPRI stress wave model

Longitudinal stress waves can be modeled using various approaches. First, the longitudinal stress wave model was implemented using a digital waveguide that was based on a digital comb filter. This implementation is valid for approximating stress waves at the boundary points of the system with a constant geometry without any impedance changes along the drill steel. During the KAPRI project the longitudinal stress wave model was re-implemented using a different digital waveguide approach (Smith, 1992) where drill steel is discretized along its length and diameter according to the model presented in Dutta (1968). This approach enables possibility to use multiple observation points along the drill steel. Main features of the KAPRI model for the longitudinal stress waves is presented in Figure 5.1. The input of the KAPRI model is similar to the simple longitudinal model where an input sequence vector was used as system excitation. The KAPRI model supports variable geometry of the drill steel, this can be used to model i.e. cascade of drill steels. The resolution of the model geometry accuracy is dependent on the model discretization intervals.

5.1.1 Direct Filter Implementation

The longitudinal waveguide consists of a constant delay line and a fractional delay filter which was used to fine-tune the longitudinal modal frequencies to the computational values determined by Eq. 3.5. The fractional delay part was implemented using a 7th order Lagrange interpola-
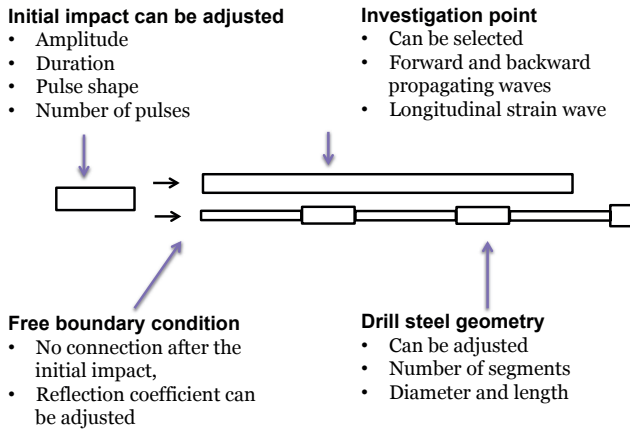
Figure 5.1. Main features of the KAPRI longitudinal stress wave model.

tion filter. The filter coefficients are determined by:

$$H_{\mathrm{FD}}(n) = \prod_{k=0, k \neq n}^{N} \frac{D-k}{n-k} \quad \text{for} \quad n = 0, 1, 2, \ldots N,$$ (5.1)

where D is the desired fractional delay and N is the filter order.

The model is implemented in Matlab using `filter` command using following transfer function

$$H(z) = \frac{1}{1 + kz^{-n}},$$ (5.2)

where k is the reflection coefficient at the bit rock interface and n is the delay line length according to model tuning. In case a fractional delay is required, the transfer function of the fractional delay filter is placed to the feedback part of the transfer function. The additional phase delay caused by the fractional delay filter must be compensated by reducing the length of the delay line n accordingly.

5.1.2 Dutta's Model for Longitudinal Strain Waves

The main principle of the waveguide model is presented in Figure 5.2(a) where a piston is modeled[1]. The forward going waves are marked with symbol B and backward propagating waves are marked with symbol A. Reflections at the impedance boundaries are also marked to the graph. The model was implemented using a sample-based algorithm where an

---

[1]In Dutta (1968) the context of the study was to investigate pulse waveforms generated by various piston designs. The piston shape is modeled to estimate the pulse shape assuming that the drill steel has infinite length and there are no reflections from the steel end at the model output.

individual point along the drill steel can be observed by summing up the forward going and the backward propagating waves. A more detailed version of the original Dutta's model is presented in Figure 5.2(b) where a piston is discretized to a forward going vector F and a backward propagating vector E. There are also two auxiliary storage vectors X and Y that are required to store the previous states of the vectors E and F.
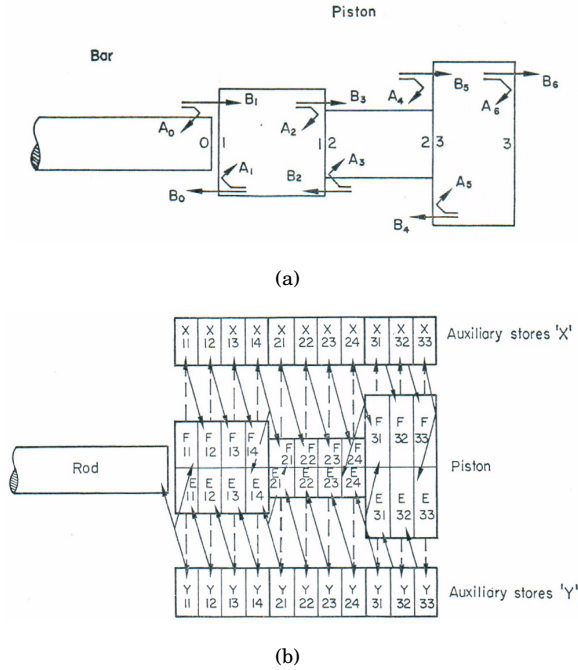
Figure 5.2. Dutta's model realization. (a) Forward going A and backwards propagating B stress waves and reflections at the impedance boundaries. (b) Model discretization and data vectors for software implementation (Both figures Adopted from Dutta (1968)).

The DWG model for the longitudinal stress waves supports an individual diameter value for each discretization point. The transmission and reflection coefficients at the cross-section boundaries are determined using Eq. 3.7. The boundary conditions at the struck end of the drill steel and at the bit-rock interface can be adjusted. Currently the reflection coefficient at the struck end of the drill steel is set to a constant value ($R_c = -1$). This represents a situation where no contact is present between piston and shank adapter at the struck end of the drill steel.

The strain waves can be inspected at a given point of the drill steel geometry. An example of model geometry is presented in Figure 5.3(a) where a drill steel is visualized. The observation point is marked with a red solid line. The model outputs, forward going stress wave in Figure

(a)

(b)

(c)

(d)
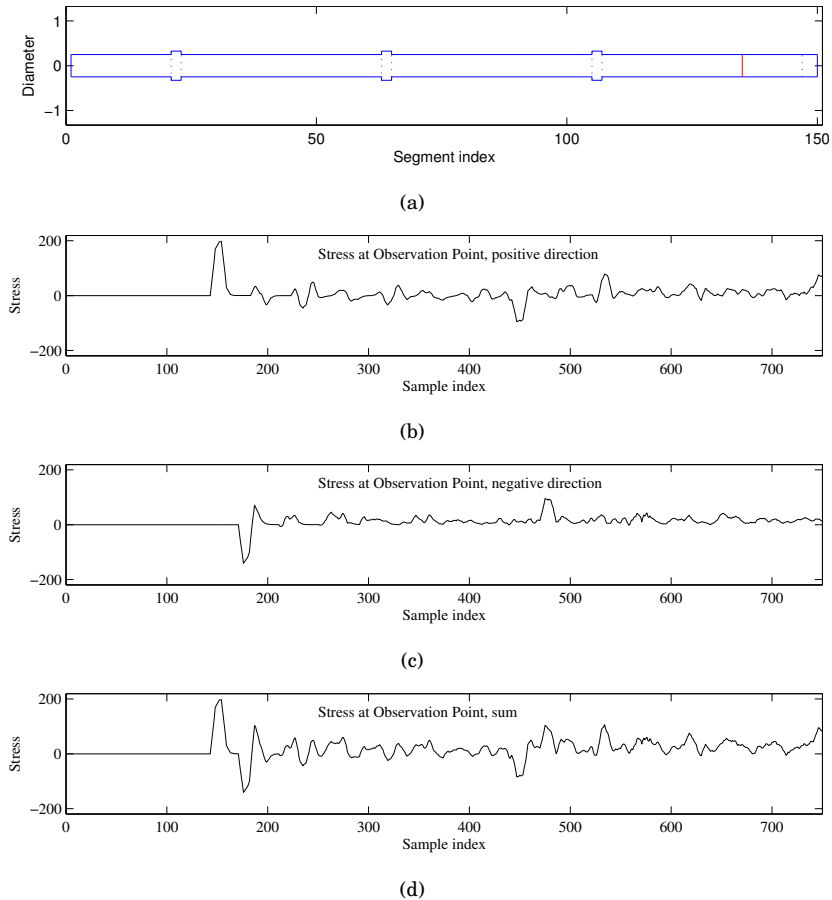
Figure 5.3. (a) Model geometry of the drill steel system, investigation point is marked with a red solid line. The excitation pulse is applied to the left end of the drill steel. (b) Modeled stress wave moving from left to right (positive direction) at the observation point. (c) Modeled stress wave moving from right to left (negative) at the observation point. (d) Sum of the positive and negative wave.

5.3(b), the backward propagating stress wave in Figure 5.3(c), and the summed version of stress waves in Figure 5.3(d). The summed version corresponds to the stress waves that can be measured from a real drill steel using strain gages.

(a)

(b)

(c)
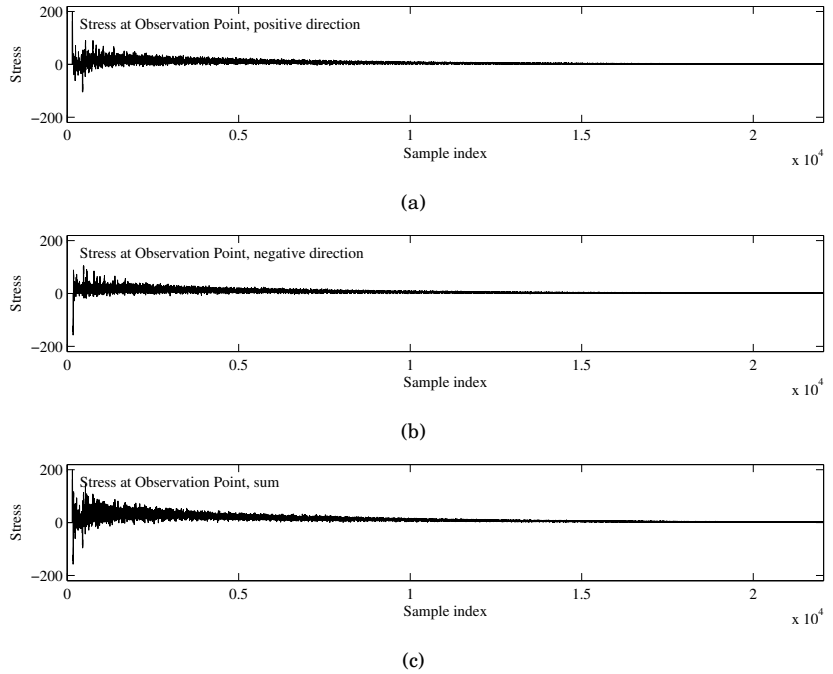
Figure 5.4. (a) Modeled stress wave moving from left to right (positive direction) at the observation point. (b) Modeled stress wave moving from right to left (negative) at the observation point. (c) Sum of the positive and negative wave.

5.2 Transversal Stress Wave Modeling

5.2.1 Dispersion Filter Design

FIR-Approach

The transversal waves are known to be dispersive. The dispersion curve is derived from the frequency dependent wave speed equation (Eq. 3.4). The dispersion filter design procedure follows the FIR filter approach described in Lehtonen (2008) where dispersion filter is constructed based on IFFT of the desired magnitude and phase responses.

An example of the desired magnitude- and phase responses is given in the upper plot in Figure 5.5(a). The magnitude spectrum is not flat through the frequency axis. The notch beginning above the desired maximum frequency ensures real-valued frequency coefficients. The phase response is designed based on the desired phase response of the target and has its sign changed above the Nyquist frequency to form complex conjugate pole pairs (See Fig. 5.5(a), lower plot).

45
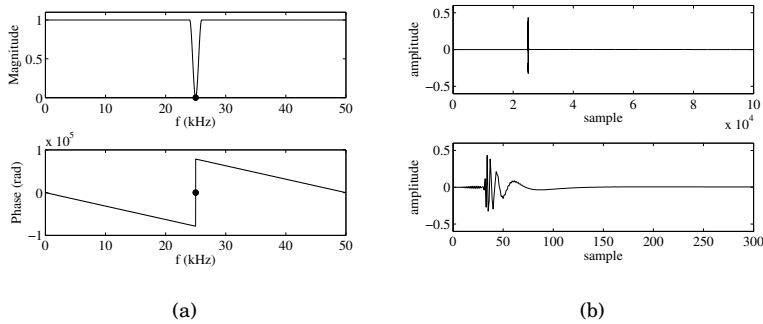
Figure 5.5. Dispersion filter design parameters: (a) Designed magnitude response of the dispersion filter (fs=50 kHz) in the upper plot. Designed phase response curve in the lower plot. (b) Dispersion filter impulse response achieved by applying IFFT to the designed magnitude and phase responses.

The resulting filter is presented in the upper plot in Figure 5.5(b) where entire IFFT sequence is plotted. The actual filter is formed by selecting values around the actual impulse so that desired total delay and desired frequency characteristics are met. An example of a truncated impulse response is presented in lower plot in Figure 5.5(b).

The resulting dispersion filter phase delay characteristics are presented in Figure 5.6. It can be seen that designed filter is very closely matched to the target at frequencies above 30 Hz. The phase delay performance at frequencies below 30 Hz is quite limited. The performance is mainly limited by the filter truncation which must be done to ensure the overall delay line length. If one wants to design a dispersion filter which is more accurate at lower frequencies the overall delay line length would ultimately be much greater than what it is required for normal sized drill steels. On the other hand it seems that sound output generated by transversal waves at lower frequencies is not critical compared to overall sound output at frequencies above 100 Hz.

Preliminary Tests With a Cascade of Allpass Filters

Another method for implementing a dispersion filter is to use first-order allpass filters. The phase-response of a first-order allpass filter can be adjusted by a single coefficient. The amount of dispersion can be increased by cascading such filters. Based on the preliminary tests the allpass cascade is realizable for the dispersion filter design. However, the phase response achieved by this method does not meet the design target of a steel bar. The target phase response has significantly large phase delay,
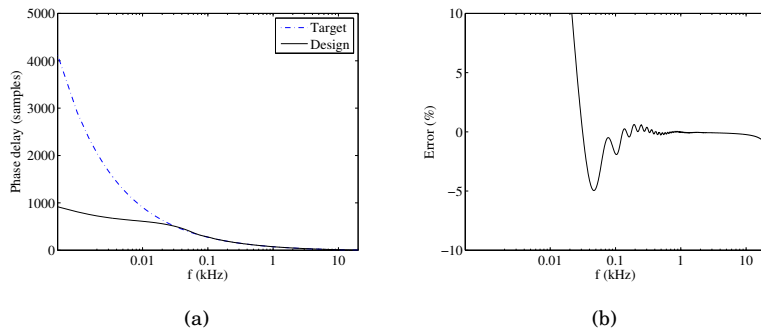
Figure 5.6. Dispersion filter phase properties: (a) Phase delay comparison between target response and designed filter. (b) Relative error percentage between the target design and the designed filter.

approximately from 1000 to 1500 samples, at lower frequencies and phase delay of 20 to 40 samples at high frequencies. The phase response curve of first-order allpass filter has either too much delay at high frequencies or too little delay at low frequencies.

Although the cascade of allpass filters is not suitable for exact modeling of the transversal vibrations it is still useful in the sound synthesis applications. An example of the method is employed in Oksanen et al. (2013b), where the cascade of allpass filters are applied to jackhammer tool sound synthesis.

5.3 Excitation Modeling

The model excitation is based on the user defined input vector. The vector can include arbitrary impulse shapes. The most simple excitation type is the rectangular pulse that closely resembles the pulse shapes in hydraulic drilling. However, the rectangular pulse is lowpass filter that suppresses the high frequency content. In cases where flat input pulse spectrum is required a single impulse is a suitable option. A windowed rectangular pulse can also be used to avoid spectral leaking caused by sharp edges in the time-domain signals.

5.4 Modeling of the Sound Generation

The sound generation of a struck bar is presented in Akay et al. (1983). This solution is based on the finite element model of the bar. The vibrat-
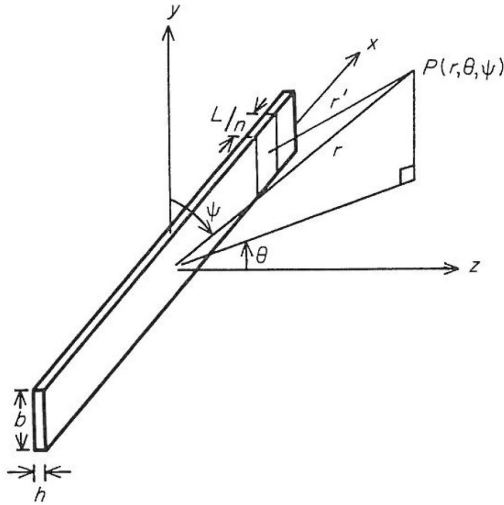
Figure 5.7. Model for sound radiation of impacted beam structure after Akay et al. (1983). The receive point P can be selected arbitrarily.

ing bar is modeled using acoustic dipole sources placed along the vibrating bar (see Fig 5.7). The resolution of the system is dependent on the number of the sources. The approach is also valid for DWG implementation where individual points along the rod can be examined. Hawkes and Burks (1979) presented the relationship between the stress waves and surface vibrations. According to this the sound radiation can be modeled by modeling the stress waves at the DWG model and then using relations presented in Hawkes and Burks (1979) to estimate surface vibration velocities that are required to set the combination of acoustic dipole sources.

6. DWG Model Implementation – from a Software Perspective

6.1 Implementation

The stress wave model implementation is divided to two main approaches, longitudinal and transversal. The main effort during KAPRI was to focus on the longitudinal model and the transversal model development was a refinement of the existing transversal model.

All models were developed in the Matlab-environment. Some parts of the longitudinal model were developed in C and were later transformed to Matlab compatible with MEX-files.

6.1.1 Longitudinal Stress Wave Model
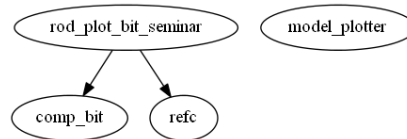
Figure 6.1. Code hierarchy for longitudinal model.

The longitudinal strain wave model code hierarchy is presented in Fig. 6.1. The main file of the implementation is a script `rod_plot_bit_seminar`. This script demonstrates the KAPRI digital waveguide model functionality.

rod_plot_bit_seminar

The model input can be determined using following variables `cycles`, `imp_dur`, `input_amplitude`, `series`, and `imp_dev`. The model geometry has two preset values, one for the cascade of drill steels with shank adapter and drill bit. The other one is used to demonstrate single steel
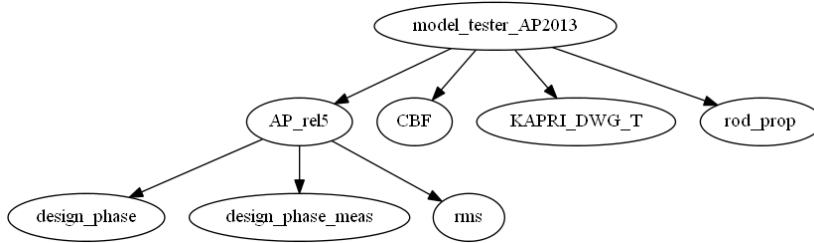
Figure 6.2. Code hierarchy for transversal model

such as the breaking hammer tool.

The script launches a visualization of the given geometry. The user can select a desired point of interest by clicking the left mouse button. Another plot will be launched where computed strain waves at the point of interest is being plotted. This plot is constructed on six subplots where positive and negative direction travelling strain waves are plotted along the summed version of them. Left hand side has a zoomed version of the beginning of the model output and the right hand side has a plot of the whole response.

The demo can be stopped by pressing the right mouse button on a desired point of the steel geometry. The simulated data can be saved by setting the sdata to value 1. The resulting file `plot_data.mat` is a struct array containing the simulation data of the selected points. The simulation results can be visualized using the `model_plotter.m` script.

comp_bit

This function performs the digital waveguide based strain wave computation for given geometry vectors. The model implementation is based on a MEX-file written in C. The model output covers strain waves fed to the bit (out_end) and strain waves propagating to positive (out_pos) and negative (out_neg) directions at the given point x. The model is based on Dutta (1968).

ref_c

This MEX-file is used to determine the reflection and transmission coefficients of a given geometry. Indexing of the coefficients is based on the notation presented in Dutta (1968).

6.1.2 Transversal Stress Wave Model

The code structure of the transversal stress wave model implementation is presented in Figure 6.2. The implementation is realized by determining the resonance frequencies of a given bar geometry. The phase-response of the dispersion filter is given by the resonance frequencies. The transversal stress wave model is implemented using a comb filter with desired reflection coefficient.

design_phase and design_phase_meas

These functions are used to design a desired phase-response based on a given rod properties. The phase-response design is based on an approximation that phase is delayed by 2π at every resonance frequency. The function output is the designed phase-response curve in radians. Difference between these functions is that design_phase is based on theoretical resonance frequencies and the design_phase_meas on the measured resonance frequencies.

AP_rel5

This function designs a FIR allpass-like filter with desired dispersion characteristics. Dispersion filter design procedure is presented in Lehtonen (2008). The implementation is based on the computational phase-delay of a steel bar or measured modal frequency of the bar.

KAPRI_DWG_T

This is the transversal stress wave model implementation based on a comb filter. The model is based on the provided dispersion filter impulse response, reflection coefficient, and input signal vector.

model_tester_AP2013

This script demonstrates transversal stress wave model. The model can be determined based on the drill steel physical properties or based on the measured transversal modal frequencies. The script plots comparison between measured and computational modes. After the modeling model output is plotted in spectral- and time-domains. The phase properties are also plotted. Sound output is also provided.

rms, CBF, and rod_prop

These are support functions that are used in transversal stress wave model. The rms computes the RMS-value of the input vector. The CBF is used to determine transversal wave speed at given frequency and geometry. The theory is based on Hawkes and Burks (1979). The rod_prop determines the transversal resonance frequencies of a given steel bar.

6.2 Model User Interface: Analysis, Plotting and Data Save Procedure

Model user interface is currently a Matlab script where user can modify existing model geometries or generate new ones. The user can also change simulation parameters from the script header. Plotting is enabled in the scripts. The longitudinal stress wave model makes it possible to save the simulation output to a separate mat-file that contains a struct-array of the simulation point data.

6.3 Model Control Parameters

The model control parameters are listed in Tables 6.1 and 6.2 . The control parameters can be changed from the individual Matlab-files.

Table 6.1. Control parameters for the longitudinal stress wave model.

Parameter name	Description
cycles	Total number of computational cycles
imp_dur	Impact duration in samples
input_amplitude	impact amplitude
series	Type of excitation, 1 = series of impacts, 0 = single impact
imp_dev	Space between consecutive impacts in samples
rod	Model geometry, 1 = cascade with couplings, bit and shank adapter, 0 = single steel
ref_hammer	Constant reflection coefficient at hammer end
sdata	Data save switch, 1 = save simulation data, 0 = do not save
l_steel	Length of a drill steel in samples
d_steel	Diameter of a drill steel
l_joint	Length of a coupling sleeve in samples
d_joint	Diameter of a coupling sleeve
l_bit	Length of a drill bit in samples
d_bit	Diameter of a drill bit
l_shank	Length of a shank adapter in samples
d_shank	Diameter of a shank adapter
n	Number of drill steels in cascade

Table 6.2. Control parameters for the transversal stress wave model.

Parameter name	Description
fs	System sample rate
dur	Output duration is seconds
series	Type of excitation, 1 = series of impacts, 0 = single impact
Lr	Length of a drill steel in meters
D	Diameter of a drill steel in meters

7. DWG Model Verification

7.1 Modeling Presets

Model verification is done by starting the simplest geometry, a single steel bar, and later increasing the model complexity by adding a more complex model geometry. The model properties for the longitudinal components are f_s = 192 kHz, Y = 220 GPa, $\rho = 7800$ kg/m^3, input amplitude 200 MPa, and input duration 10 samples ≈ 0.0521 ms.

Figure 7.1 presents an example of the modeled stress waves. Forward going (positive direction) stress wave is presented in Figure 7.1(a). Backwards propagating wave is presented in Figure 7.1(b). The model stress wave output is achieved by summing up the positive and negative direction stress waves (Figure 7.1(c)). The sum wave is similar to the one that can be observed using a pair of strain gages mounted on the opposite sides of the steel bar.

7.2 Breaking Hammer Tool

7.2.1 Uniform Steel

An example of the simple geometry is presented in Figure 7.2 where a single steel bar is presented. This design can be used to model the breaking hammer tool. The length of the steel bar is approximately 1.1 m and diameter is approximately 0.08 m. The observation point is marked with a red dash dot line. The observation point can be varied along the steel.

Time-domain model output is presented in Figures 7.3(a) and 7.3(b) the first is a zoomed version and the latter one is the overall response. The ini-
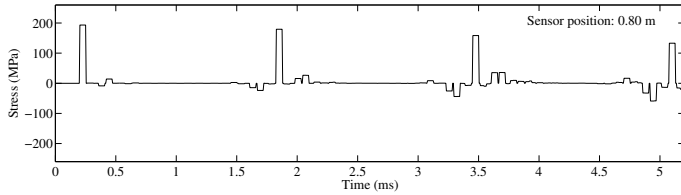
(a)
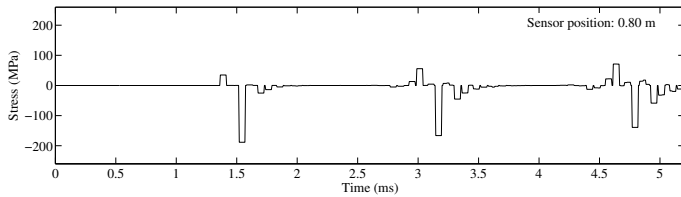
(b)
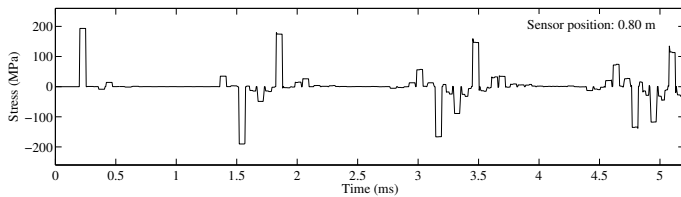
(c)

Figure 7.1. Example of modeled stress waves. (a) positive direction propagating stress wave (left – right), (b) negative direction propagating stress wave (right – left), and (c) sum of the stress waves.
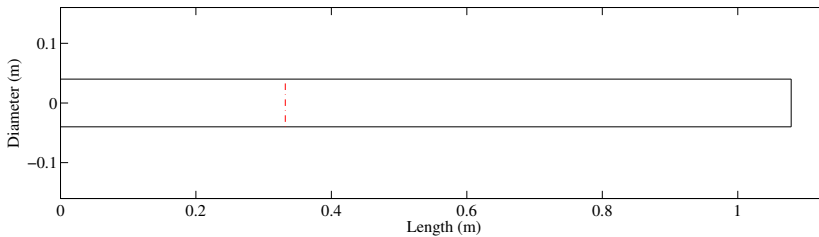
Figure 7.2. Steel bar geometry. Initial impact point is the left end of the bar. Instrumentation point is marked with a dash dot line.

tial pulse can be seen between 0.1 – 0.2 ms. First inverse reflection from the rock end is approximately at 0.4 ms and first reflection from the hammer end at approximately 0.55 ms point. The model decay coefficient is used to fine tune the model output to desired decay time. The spectrum of the model output is presented in Figure 7.3(c). The computational longitudinal resonance frequencies are plotted with dotted lines. The spectrum is normalized so that the maximum value is set to 0 dB level. Magnitude of an individual mode is affected by the observation point. There can be

Figure 7.3. Model response with a linear boundary condition. (a) Time-domain response (0–0.65 ms) . (b) Time-domain response. (c) Output spectrum, computational resonance frequencies are plotted with dashed lines.

seen an example of the cancelled modal component at around 19 kHz region.

7.3 Rock Drill Model

7.3.1 System With One Drill Steel

Another approach for the stress wave modeling was to use it to drilling equipment. An example of a drill system is presented in Figure 7.4. Starting from left to right the first part of the system is a shank adapter that is attached to the coupling sleeve. The drill steel is followed after the coupling sleeve and the model is concluded with a drill bit.

The model output of the system is presented in Figures 7.5(a) and 7.5(b). The initial impulse can be seen at around 0.1 ms. The pulse shape is smeared because of the reflections caused by the impedance change between the shank adapter and coupling sleeve. The first positive reflection is caused by the impedance change between the coupling sleeve and the drill steel. The second positive reflection around 1.4 ms is caused by the

57
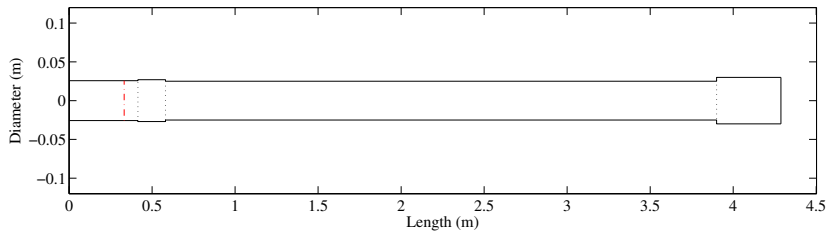
Figure 7.4. Simple drilling system geometry consisting of shank adapter, coupling sleeve, drill steel, and drill bit.

impedance change between the drill steel and the bit. The first reflection from the free end boundary is around 1.6 ms and the reflection from the hammer end is around 1.8 ms.

Spectrum of the model output is presented in Figure 7.5(c). The resonance peaks are well aligned with the computational resonance frequencies that are marked with dotted lines. There can be seen an example of a cancelled mode at the proximity of 15.5 kHz. Spectral envelope fluctuation is caused by the spatial nodal positions around the end of the rod. If the observation point would have been selected differentially the modal positions would be at same positions but the spectral envelope would have different shape.

The output spectrum is presented in Figure **??**. Compared to the output spectrum of the free end boundary case (Fig. 7.5(c)) the energy is distributed more evenly around the spectrum. The modal positions have also moved up in frequency compared to the computational values. Although the effect it not as clear as with the breaking hammer tool.

7.3.2   Cascade Of Drill Steels (n=4)

To increase the model realism the drill steels were connected to a cascade as seen with the rock drilling equipment. The model geometry for the cascaded drill steels is presented in Figure 7.6. The model is mainly similar to the previous case but the number of drill steels and coupling sleeves are increased to four. Another difference is the placement of the observation point that is now in the drill steel instead of the shank adapter.

The time-domain response of the cascade model is presented in Figures 7.7(a) and 7.7(a). The initial impact has bit of ripple caused by the impedance changes along the cascade system (from shank adapter to coupling sleeve and from coupling sleeve to drill steel). Disturbances caused by the other drill steel joints are clearly visible around 2.5 and 4 ms. The
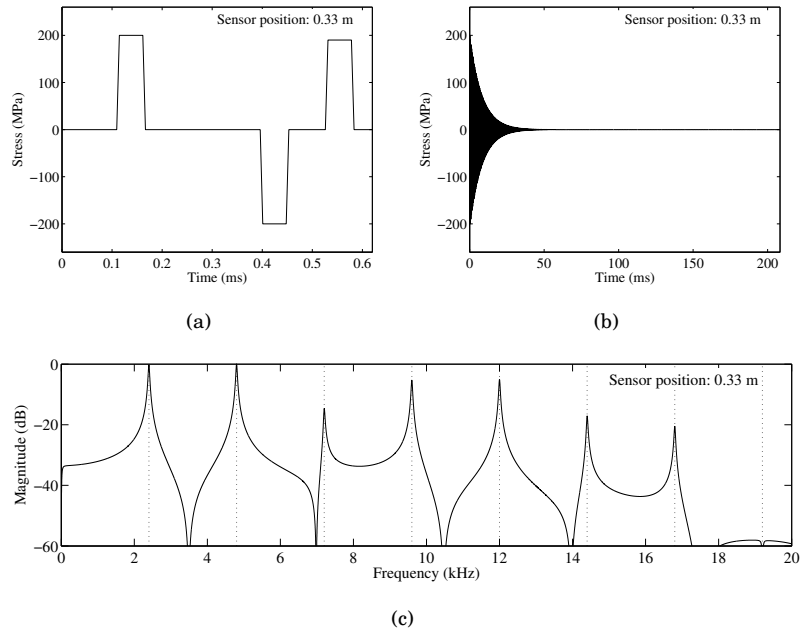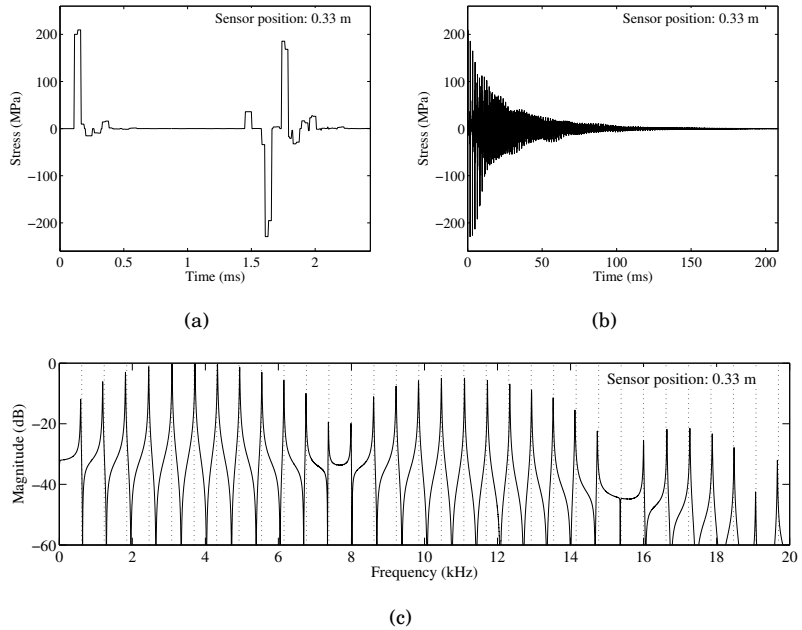
Figure 7.5. Simple drill system model response with a linear boundary condition. (a) Time-domain response (0–2.5 ms). (b) Time-domain response. (c) Output spectrum, computational resonance frequencies are plotted with dashed lines.

first positive reflection around 5 ms is caused by the impedance change between the last drill steel and the bit. The first reflection from the hammer end (free boundary condition) can be seen around 6.5 ms. The time-domain response (Fig. 7.7(b)) is decaying much slower compared to the response of the single steel model (Fig. 7.5(b)).

Spectrum of the model output is presented in Figure 7.7(c). The resonance frequencies of the cascade system are closely matched to the computational resonance frequencies (dotted lines). The spectral envelope has the fluctuating characteristics as seen from the previous spectral plots (Figs. 7.3(c) and 7.5(c)).
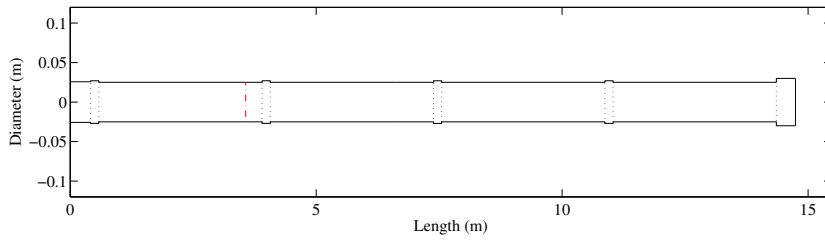
Figure 7.6. More complex drilling system geometry consisting of shank adapter, cascade ($n = 4$) of coupling sleeves and drill steels, and drill bit.

(a)

(b)

(c)
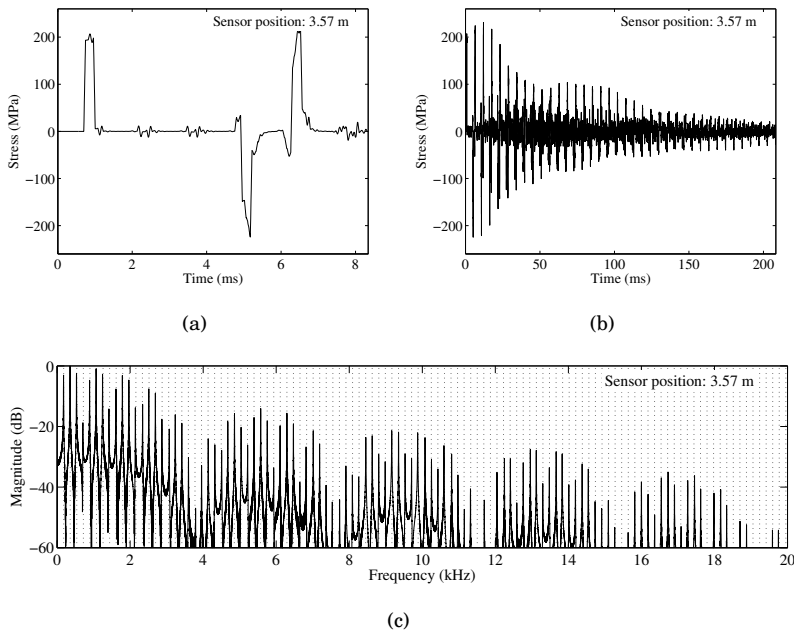
Figure 7.7. More complex drill system model response with a linear boundary condition. (a) Time-domain response (0–8.2 ms). (b) Time-domain response. (c) Output spectrum, computational resonance frequencies are plotted with dashed lines.

7.4   Transversal Stress Wave Model

Transversal stress wave model was tested by designing a dispersion filter to match steel bar dimensions. An example of the model response is described in Figure 7.8. It can be seen that modal frequencies match the design target quite closely at low frequencies $f < 3.5$ kHz, at high frequencies the model tuning is bit too high. Corresponding phase response of the dispersion filter is presented in Figure 7.9. The phase delay curve is quite closely matched to the design target at frequencies above 2 kHz.
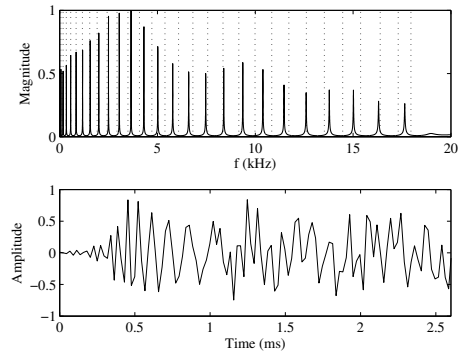
Figure 7.8. Transversal model output. (top) Model output spectrum, and (bottom) model output in time-domain.
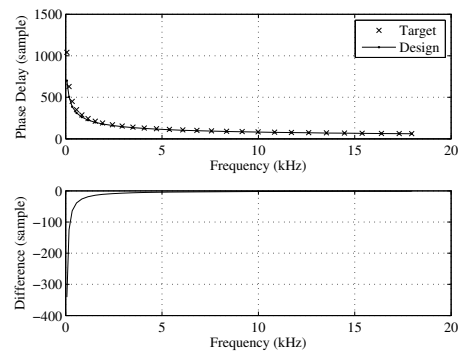
Figure 7.9. Transversal model phase response. (top) Phase response of the designed model and target values. (bottom) Difference in phase response between target and model responses.

8. Acoustical Analysis of Excavated Tunnels in Rock

8.1 Acoustical Measurements

The measured space is a teaching and test tunnel located at the Aalto University campus, see Fig. 8.1. The characteristics of the tunnel match closely the ones at excavation and underground construction sites. The tunnel floor consists of a layer of gravel on top of the bedrock. Parts of the tunnel walls and ceiling are reinforced with sprayed plaster coating, but the majority of the wall area is bare and extremely uneven rock.

Figure 8.1. Overall view of the main practice drilling tunnel. The sound source was located at the far end of the tunnel and receiver locations varied along the tunnel.

The acoustic properties of the space were determined using the standard log-sweep method Farina (2000); Müller and Massarani (2001). A sound source is located at a certain position within the tunnel, and a set of logarithmic sine sweeps are played. The acoustic response to this sweep is measured using a microphone positioned at a pre-determined location,
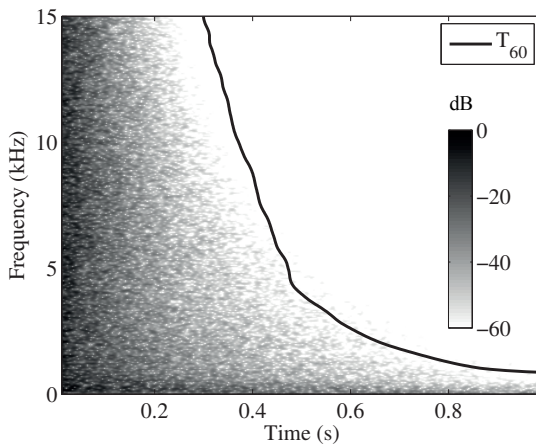
Figure 8.2. Spectrogram of the measured impulse response and estimated T_{60} value.

at a great enough distance to be well within the reverberant soundfield. Sound signal playback and recording were carried out with custom made software in Matlab. Log-sweep duration was 10 s and frequency range was 20 Hz to 20 kHz. The excitation signal was repeated five times in each speaker and receiver position to help avoid sources of random error.

The excitation signals were produced using a stand-mounted active loudspeaker (Genelec 1032A). To approximate an omnidirectional acoustic excitation with the directional speaker, the measurements were conducted in seven different speaker orientations and averaged. The set of speaker orientations consisted of six positions in the horizontal plane 60 degrees apart from each other and one where loudspeaker was pointing upwards. The response measurements were also carried out using a passive omnidirectional loudspeaker. The omnidirectional loudspeaker was limited in efficiency and was not capable of producing the high SPLs required at greater distances, so the omnidirectional measurements were used to verify the results produced by the directional speaker.

Acoustic responses were measured using a pressure-field microphone (B&K 4192) and a B-format Soundfield microphone (ST 350) simultaneously. The microphones were placed approximately 1.5 m above the floor and close to the axial line of the tunnel. The distance between microphones was approximately 30 cm. The distance of the receiver point from the sound source was varied from 5 m to 20 m.

The impulse response of the space is derived from the measured responses by convolving it with the time reversed version of the excitation signal. The impulse responses are then time-aligned and averaged

with the other appropriate measurements. In the case of the directional speaker, this is all repeated for measurements at the seven different angles for a particular distance between sound source and receiver. In the omnidirectional speaker case, this is just the repeated measurements made at that distance.

8.2   Analysis of Measured Responses

The first step of analysis was to compare the responses produced by the average of directional speaker responses with those produced by the omnidirectional speaker. The results produced agree closely enough to suggest that the average of directional speaker responses is a good approximation, especially within the horizontal plane. The omnidirectional speaker has a poor response below around 100 Hz, and so verification is not possible below that frequency. However, at this frequency the directionality of the Genelec 1032A is less pronounced, so we assume that the approximation holds.

Figure 8.2 shows a spectrogram of the response produced using the average of directional speaker responses, taken at a distance of 13m between source and receiver. The response is created from the B-format signal recorded at the Soundfield microphone by creating a virtual microphone pointing towards the source. Overlayed on the spectrogram is the estimated T_{60} with respect to frequency. Inspection of the spectrogram shows that the response consists of only diffuse sound, with no clear discrete echoes visible.

Figure 8.3 shows relative T_{60} times of the responses produced by calculating eight different virtual microphones from the B-format signal, pointing in eight directions distributed evenly around the circle. It should be clear from inspection that there is a fairly significant variation of frequency dependent reverberation time with direction.
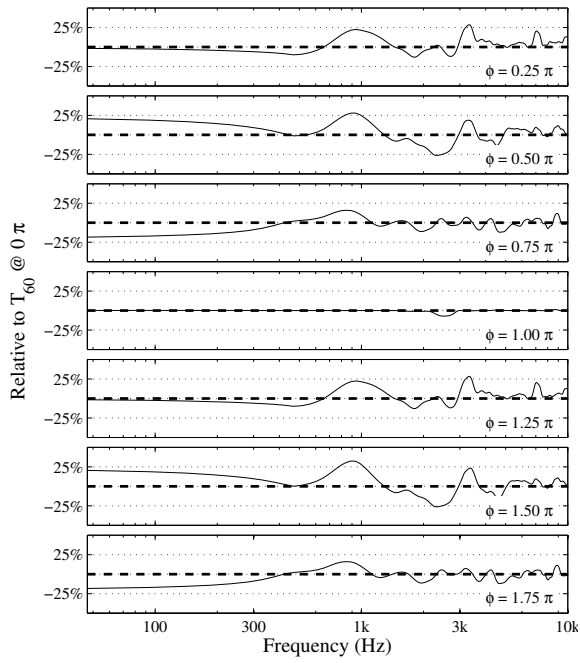
Figure 8.3. Relative difference in T_{60} with respect to direction ϕ.

9.   Summary and Conclusions

9.1   Summary

This report describes research activities during KAPRI project. At first, a literature study was conducted. In this study the topics covered were drill steel vibrations, stress wave generation in drill steels, modeling of the vibration phenomena of steel bars and percussive drilling noise reduction. Based on the literature review a brief introduction to the steel bar vibrations was introduced.

Then the vibrations in steel bars were analyzed under laboratory conditions using strain gages, microphones and laser Doppler vibrometer. The laboratory analysis showed that basic theories of the stress waves and vibrations were valid. Although the analysis conducted under laboratory conditions was lacking the realism of the actual drilling the analysis revealed plenty of knowledge on the vibration phenomena and related sound generation. The laboratory analysis was carried out in acoustically treated facilities, anechoic chamber, where reflections from the space is minimized and the measured responses contain only the sounds generated by the vibrating steel bar.

After the vibration analysis computational models were developed to mimic the stress wave behavior in the struck metal bars. The computational models were divided into two categories based on the wave polarization, longitudinal and transversal. The longitudinal model was implemented using digital waveguide structure with reflecting boundaries at impedance changes.

The transversal stress waves were modeled using a comb filter with a constant reflection coefficient. The dispersion was implemented using a FIR filter that had flat frequency response almost to the Nyquist

limit. The frequency response was decaying towards Nyquist limit where it had value of zero. The dispersion was modeled by designing the desired phase response in the frequency domain and the resulting filter impulse response was achieved by taking IFFT of the frequency- and phase responses.

The model implementation was also investigated from the software perspective. The code structure was explained and model control parameters were introduced. The models were implemented with Matlab. The longitudinal stress wave model and the nonlinear bit-rock interface were written in C and were later compiled to Matlab compatible MEX-files.

The computational models were tested against the theoretical values in time- and frequency domains. The longitudinal model is capable to model complex steel bar geometries and the nonlinear bit-rock model is capable to reproduce time-domain signals that are presented in the literature. The transversal model seems to be able to reproduce vibrations in a single steel bar. Transversal wave behavior at the impedance boundaries remains still unknown.

A small study was conducted to find out acoustical conditions in excavated tunnels in rock. The study was conducted in the training tunnel at Aalto University. The analysis consisted of the standard swept-sine method that was used to model tunnel impulse response at various locations along the tunnel. The analysis was extended to cover directional features of the reverberation. Based on the analysis results an efficient directional reverberator method was developed. The method is not described in this report, but is presented in detail at Oksanen et al. (2013a).

9.2 Main Results

1. Literature study pointed out many relevant sources to prior studies. It seems that most of the basic research on the topic has been conducted from 1960s to 1980s.

2. During the project plenty of knowledge was gained in the field of laboratory analysis of the vibration steel bar vibrations.

3. Digital waveguides were found out to be suitable and computationally effective solution for longitudinal stress wave modeling. A robust Matlab toolbox for stress wave analysis was developed and tested during project.

4. Transversal stress waves can be modeled to some extend using FIR based dispersion filter in a comb filter. Cascade of first-order allpass filter was also tested and was found out that it is possible to use this approach in the field of sound synthesis Oksanen et al. (2013b).

5. Acoustical analysis of the excavated tunnels was conducted. The results show that reverberation is such conditions is diffuse by nature. Compared to typical rooms where there are plenty of early reflections the excavated tunnels had very diffuse reverberation. The directional study of the reverberation was also conducted and gained results can be utilized in the field of noise control.

Bibliography

J. S. Abel, V. Välimäki, and J. O. Smith. Robust, efficient design of allpass filters for dispersive string sound synthesis. *IEEE Signal Processing Letters*, 17(4): 406–409, april 2010.

A. Akay. A review of impact noise. *Journal of the Acoustical Society of America*, 64(4):977–987, 1978.

A. Akay, M. Bengisu, and M. Latcha. Transient acoustic radiation from impacted beam-like structures. *Journal of Sound and Vibration*, 91(1):135–145, 1983.

T. Barnes and B. Kirkwood. Passbands for acoustic transmission in an idealized drill string. *Journal of the Acoustical Society of America*, 51(5B):1606–1608, 1972.

P. Berzi, R. Beccu, and B. Lundberg. Identification of a percussive drill rod joint from its response to stress wave loading. *International Journal of Impact Engineering*, 18(3):281–290, 1996.

S. Bilbao. *Numerical Sound Synthesis: Finite Difference Schemes and Simulation in Musical Acoustics*. John Wiley & Sons, 2009.

I. Carlvik. The generation of bending vibrations in drill rods. *International Journal of Rock Mechanics and Mining Sciences & Geomechanics Abstracts*, 18(2):167–172, 1981.

C. W. De Silva. *Vibration – Fundamentals and Practice*. CRC press LLC, 1999.

O. K. Demir. Assessment of hand-type hammer drill bits under percussive loading. Master's thesis, Middle East Technical University, Ankara, Turkey, 2007.

N. Dongmin. Rigid impact – the mechanism of percussive rock drilling. In *Proceedings of the 42nd US Rock Mechanics Symposium*, pages 1–5, San Francisco, USA, June 29th – July 2nd 2008. Paper ID 08-075.

D. S. Drumheller. Wave impedances of drill strings and other periodic media. *Journal of the Acoustical Society of America*, 112(6):2527–2539, 2002.

P. K. Dutta. The determination of stress waveforms produced by percussive drill pistons of various geometrical designs. *International Journal of Rock Mechanics and Mining Sciences & Geomechanics Abstracts*, 5(6):501–510, 1968.

P. K. Dutta, J. Burks, and R. C. Bartholomae. Measurement and analysis of the stress wave generated rod noise in percussive rock drill. In *Paper - SESA (Society for Experimental Stress Analysis)*, pages 218–226, 1981.

V. Erem'yants and A. Slepnev. Strain waves in colliding bars having nonparallel faces. *Journal of Mining Science*, 42(6):587–591, 2006.

D. J. Ewins. *Modal testing: theory, practice, and application*. Research Studies Press, 2nd. edition, 2000.

A. Farina. Simultaneous measurement of impulse response and distortion with a swept-sine technique. In *108th AES Convention*, Paris, France, Feb. 2000.

N. H. Fletcher and T. D. Rossing. *The physics of musical instruments*. Springer-Verlag, 1991.

K. F. Graff. *Wave motion in elastic solids*. Dover books on engineering. Dover Publications, 1975. Reprint 1991.

I. Hawkes and J. Burks. Investigation of noise and vibration in percussive drill rods. *International Journal of Rock Mechanics and Mining Sciences & Geomechanics Abstracts*, 16(6):363–376, 1979.

I. Hawkes and P. K. Chakravarty. Strain wave behavior in percussive drill steels during drilling operations. *Mine & Quarry Engineering*, 27(3):318–326 and 367–373, 1961.

L. Hillström and B. Lundberg. Analysis of elastic flexural waves in non-uniform beams based on measurement of strains and accelerations. *Journal of Sound and Vibration*, 247(2):227–242, 2001.

Z. Kaczmarek. Elastic bar transfer function determination using two-point strain measurements. *IEEE Transactions on Instrumentation and Measurement*, 58 (1):147–151, Jan. 2009.

Kyowa Electronics Instruments CO., LTD. What's a Strain Gauge? – Introduction to strain gages. Product manual, 2011. URL www.kyowa-ei.co.jp/english/products/gages/pdf/whats.pdf. Accessed Thursday 19th December, 2013.

T. I. Laakso, V. Välimäki, M. Karjalainen, and U. K. Laine. Splitting the unit delay. *IEEE Signal Processing Magazine*, 13(1):30–60, Jan. 1996.

H.-M. Lehtonen. Analysis of piano tones using an inharmonic inverse comb filter. In *Proceedings of the 11th Int. Conference on Digital Audio Effects (DAFx-08)*, pages 333–340, Espoo, Finland, September 1–4, 2008.

C. Lesage, R. Oddo, Y. Champoux, and N. Atalla. Experimental characterization of the noise generation mechanism of percussion drill rods. *CIM Bulletin*, 90 (1010):65–69, 1997.

X. Li, T. S. Lok, D. A. Summers, G. Rupert, and J. Tyler. Stress and energy reflection from impact on rocks using different indentors. *Geotechnical and Geological Engineering*, 19:119–136, 2001.

N. Lous, S. Rienstra, and I. Adan. Sound transmission through a periodic cascade with application to drill pipes. *Journal of the Acoustical Society of America*, 103 (5):2302–2311, 1998.

B. Lundberg. Microcomputer simulation of stress wave energy transfer to rock in percussive drilling. *International Journal of Rock Mechanics and Mining Sciences & Geomechanics Abstracts*, 19(5):229–239, 1982.

B. Lundberg. Microcomputer simulation of percussive drilling. *International Journal of Rock Mechanics and Mining Sciences & Geomechanics Abstracts*, 22:237–249, 1985.

S. Müller and P. Massarani. Transfer-function measurement with sweeps. *Journal of the Audio Engineering Society*, 49(6):443–471, 2001.

S. Oksanen, J. Parker, A. Politis, and V. Välimäki. A directional diffuse reverberation model for excavated tunnels in rock. In *Proc. IEEE international Conference on Acoustics, Speech and Signal Processing ICASSP 2013*, Vancouver, Canada, May 26–31, 2013a.

S. Oksanen, J. Parker, and V. Välimäki. Physically informed synthesis of jackhammer tool impact sounds. Accepted to be published in 16th Int. Conf. on Digital Audio Effects DAFx-13, Sept. 2–6, 2013b.

A. Roberts, I. Hawkes, and J. Furby. Transmission of energy in percussive drilling. *Mine and Quarry Engineering*, 44(7):447–458, 1962.

J. O. Smith. Physical modeling using digital waveguides. *Computer Music Journal*, 16(4):74–91, 1992.

R. Stein and W. Aljoe. Concentric drill steels for noise reduction of percussion drilling. In *Proceedings of the InterNoise 1986*, pages 333–336, Cambridge, USA, July 21–23 1986.

J. Tanttari and K. Saarinen. Iskuporauksen kankimelusta. In *Proceedings of the Akustiikkapäivät 1995*, pages 45–50, Tampere, Finland, 1995.

Appendix, Publications Produced During the KAPRI Project

Publications produced during the KAPRI project are presented in the following Sections.

I J. Parker, S. Oksanen, and V. Välimäki, "Measuring and Modelling the Reverberation of a Bare Rock Tunnel", in *Proc. of the Akustiikkapäivät 2013*, May 22–23, 2013, Turku, Finland.

II S. Oksanen, J. Parker, and V. Välimäki, "Vibroacoustic Analysis and Synthesis of Struck Metal Bars Using Musical Instrument Modeling Techniques", in *Proc. of the Akustiikkapäivät 2013*, May 22–23, 2013, Turku, Finland.

III S. Oksanen, J. Parker, A. Politis, and V. Välimäki, "A directional diffuse reverberation model for excavated tunnels in rock", in *Proc. IEEE international Conference on Acoustics, Speech and Signal Processing ICASSP 2013*, May 26–31, 2013, Vancouver, Canada.

IV S. Oksanen, J. Parker, and V. Välimäki. "Physically informed synthesis of jackhammer tool impact sounds", in *Proc of the 16th International Conference on Digital Audio Effects DAFx-13*, Sept. 2–6, 2013, Maynooth, Ireland.

A   Publication I

J. Parker, S. Oksanen, and V. Välimäki, "Measuring and Modelling the Reverberation of a Bare Rock Tunnel", in *Proc. of the Akustiikkapäivät 2013*, May 22–23, 2013, Turku, Finland.

MEASURING AND MODELLING THE REVERBERATION OF A BARE ROCK TUNNEL

Julian Parker, Sami Oksanen, Archontis Politis, and Vesa Välimäki

Aalto University, School of Electrical Engineering
Department of Signal Processing and Acoustics
P.O. Box 13000, FI-00076 AALTO, Espoo, Finland

julian.parker@aalto.fi, sami.oksanen@aalto.fi, vesa.valimaki@aalto.fi

Abstract

Acoustic impulse responses of an excavated tunnel were measured. Analysis of the impulse responses shows that they are very diffuse from the start. A reverberator suitable for reproducing this type of response is proposed. The input signal is first comb-filtered and then convolved with a sparse noise sequence of the same length as the filter's delay line. An IIR loop filter inside the comb filter determines the decay rate of the response and is derived from the Yule-Walker approximation of the measured frequency-dependent reverberation time. The particular sparse noise sequence proposed in this work combines three velvet noise sequences, two of which have time-varying weights. To simulate the directional soundfield in a tunnel, the use of multiple such reverberators, each associated with a virtual source distributed evenly around the listener, is suggested. The proposed tunnel acoustics simulation can be employed in gaming, in film sound, or in working machine simulators.

1 INTRODUCTION

Recorded impulse responses of spaces have been directly used as a means to add natural reverberation of a specific character to a dry recording, or as a way to listen how a specific space would affect a source signal, a process that in the context of architectural and virtual acoustics is termed auralisation [1]. A straightforward way to achieve that is to convolve a source signal with a recorded room impulse response (RIR), which herein is termed as convolution reverberation [1]. An alternative approach, which provides more flexibility and computational efficiency, is to estimate the most relevant parameters from a recorded RIR and then map these parameters to common reverberation algorithms, such as combinations of delay-lines and feedback delay networks [2, 1]. Common parameters are mixing times between the early and late reverberant part, arrival times and amplitudes of discrete early reflections and reverberation times of the late diffuse part [3].

In Sec. 2, we describe the measurement of the B-Format impulse response of an excavated rock tunnel, and present some analysis of its main characteristics. In Sec. 3 we present a method of approximating this reverberation for arbitrary input through a novel multi-channel sound reproduction system. In Sec. 5, we conclude.

Figure 1: *Overall view of the main practice drilling tunnel. The sound source was located at the far end of the tunnel and receiver locations varied along the tunnel. (Photo Otto Hedström)*

2   IMPULSE RESPONSE MEASUREMENTS IN A TUNNEL

The measured space is a teaching and test tunnel located at the Aalto University campus, see Fig. 1. The characteristics of the tunnel match closely the ones at excavation and underground construction sites. The tunnel floor consists of a layer of gravel on top of the bedrock. Parts of the tunnel walls and ceiling are reinforced with sprayed plaster coating, but the majority of the wall area is bare and extremely uneven rock.

The acoustic properties of the space were determined using the standard log-sweep method. A sound source is located at a certain position within the tunnel, and a set of logarithmic sine sweeps are played. The acoustic response to this sweep is measured using a microphone positioned at a pre-determined location, at a great enough distance to be well within the reverberant soundfield. Sound signal playback and recording were carried out with custom made software in Matlab. Log-sweep duration was 10 s and frequency range was 20 Hz to 20 kHz. The excitation signal was repeated five times in each speaker and receiver position to help avoid sources of random error.

The excitation signals were produced using a stand-mounted active loudspeaker (Genelec 1032A). To approximate an omnidirectional acoustic excitation with the directional speaker, the measurements were conducted in seven different speaker orientations and averaged. The set of speaker orientations consisted of six positions in the horizontal plane 60 degrees apart from each other and one where loudspeaker was pointing upwards. The response measurements were also carried out using a passive omnidirectional loudspeaker. The omnidirectional loudspeaker was limited in efficiency and was not
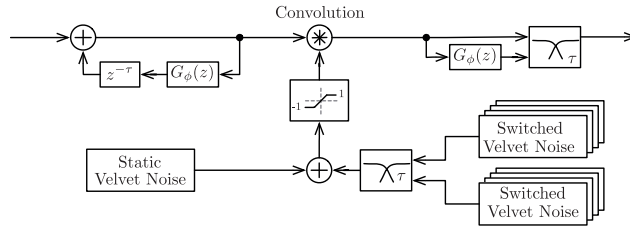
Convolution

Figure 2: *Block diagram showing structure of a single channel of the novel reverberator.*

capable of producing the high SPLs required at greater distances, so the omnidirectional measurements were used to verify the results produced by the directional speaker.

Acoustic responses were measured using a pressure-field microphone (B&K 4192) and a B-format Soundfield microphone (ST 350) simultaneously. The microphones were placed approximately 1.5 m above the floor and close to the axial line of the tunnel. The distance between microphones was approximately 30 cm. The distance of the receiver point from the sound source was varied from 5 m to 20 m.

3 NOVEL DIRECTIONAL DIFFUSE REVERBERATION MODEL

As can be seen in the analysis of the measured responses of the tunnel given above in Sec. 2, the defining characteristic of reverberation in an irregular rock tunnel is that no strong early reflections are present, only a diffuse tail. The density of echoes is also extremely high from the start of the response. The other interesting aspect of the measured reverberation is the frequency-dependent variation of T_{60} with angle. A successful model should be able to reproduce this fast onset of diffuse sound, as well as being computationally efficient enough to be used in multi-channel or spatial audio context to reproduce the directional nature of the sound field.

3.1 Single-channel velvet noise reverberation

The basic reverberation structure is similar to those presented by Lee et al. [4], with some modifications. The core idea of the approach is that the diffuse tail of an acoustic response can be approximated by convolution with exponentially decaying white noise. However, direct convolution with exponentially decaying white noise has some drawbacks – namely that it is inefficient and lacks the possibility of varying reverberation time with frequency. Instead, we can use a comb filter to produce a series of exponentially decaying repeats of the input signal, and then convolve with a shorter sequence of noise to fill the gaps. The result is very close to the direct convolution, but computationally much less expensive. Frequency dependent reverberation time can be obtained by the addition of a damping filter into the feedback loop of the comb filter.

The efficiency of such a structure can be improved further by utilizing a form of sparse noise (noise that contains many zeros) instead of Gaussian white noise. Karjalainen and Järveläinen [5] propose one such type of noise, which they call 'velvet noise'.
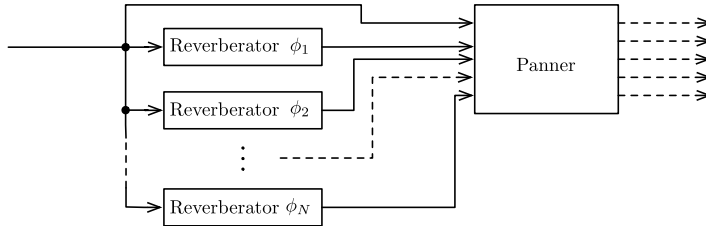
Figure 3: *Block diagram showing structure of complete multi-channel reverberator.*

This particular sparse noise possesses the desirable quality of a constant, non-lumpy distribution in time. This quality manifests itself as an audible smoothness. This density of this form of noise may be greatly reduced (down to as low as several thousand impulses per second) whilst still being audibly equivalent to Gaussian noise [5, 6].

The other major challenge of this form of reverberation is modifying the sparse noise sequence so that continuity is maintained between the sections delineated by the echoes of the comb-filter. In the case of frequency-independent reverberation time, this is simply a case of providing the noise sequence with an exponentially decaying envelope dependent on the length and damping coefficient of the comb filter. In the case of frequency-dependent reverberation time, Lee et al. [4] suggest crossfading between an unfiltered noise-sequence and the same noise sequence filtered with the damping filter.

Figure 2 shows the proposed structure of the reverberator. It consists of a comb filter of length τ samples, containing a damping filter $G_\phi(z)$. This damping filter is an IIR filter derived from Yule-Walker approximation of the frequency-dependent T_{60} of the measured tunnel response for a particular direction. The output of this comb filter is convolved with a sparse noise sequence of length τ. This sparse noise sequence is a new hybrid of the non-overlapping sequence and overlapping sequence methods described by Lee et al. [4]. Three noise sequences are generated. Firstly, a static noise sequence of low density (500 impulses per second). Secondly, two denser noise sequences (2000 impulses per second) are generated, and crossfading is performed between them over each comb-filter period τ. At the end of a comb-filter period, the first noise-sequence (where the crossfading started) is replaced by the second noise sequence, which is then in turn replaced by a newly generated noise sequence. This process repeats for every comb-filter period τ. The crossfaded noise sequence is added to the static noise sequence, passed through a hard clipper to remove the occasional occurrences of co-incident (and hence double amplitude) impulses, and then convolved with the output of the comb-filter. This combination of static and varying sparse noise was chosen as it successfully suppressed artifacts whilst still being sparse enough to keep the convolution efficient. Finally, the convolved signal is crossfaded over each period τ with a version of itself filtered by the damping filter $G_\phi(z)$, in order to approximate the correct envelope. Experimentation showed that best results were obtained when the comb-filter period is $\tau \approx 30$ ms.

3.2 Multi-channel extension of the reverberator

To extend the reverberation structure to a directional model, we make the assumption that due to the highly diffuse nature of the reflections, the sound arriving from different directions is essentially uncorrelated. We can then approximate the directional response by the use of a number of separate reverberators, each of which is treated as a virtual source within the space, and spatialized according to some established system for distribution to a loudspeaker system (see Fig. Figure 3). In this case, we use VBAP [7] to perform this spatialization. Each reverberator ϕ_n has its damping filter G_{ϕ_n} derived from the directional T_{60} time measured in the same direction as the corresponding virtual source. For the purpose of this work we employed 8 reverberators and hence 8 virtual sources, distributed evenly at increments of $\frac{\pi}{4}$ in a plane around the listener. The dry signal is also treated as a virtual source, and placed at the front of the space, to be consistent with the position of the source during the measurements. It is possible that a smaller number of virtual sources and reverberators could be used without much loss of directional information due to the limited angular resolution of the B-Format microphone.

4   RESULTS

Figure 5 shows a spectrogram and T_{60} estimate of the response produced using the average of directional speaker responses, taken at a distance of 13m between source and receiver. The response is created from the B-format signal by creating a virtual microphone pointing towards the source. Inspection of the spectrogram shows that the response consists of only diffuse sound, with no clear discrete echoes visible. Figure 5 shows spectrogram of the impulse response of the first reverberator (and hence first virtual source) in the model described above. The first reverberator is placed at zero angle (i.e. straight ahead). This response can be compared to the measured response given in Figure 5, which is the response to which the frequency dependent reverberation of this particular reverberator has been fitted. The diffuse nature of the reverberation seems to have been captured correctly, and the T_{60} is approximated well.

The model was tested with a variety of input sounds, on an 8.1 surround audio system in a listening room conforming to the ITU-R BS.1116 standard. The resulting sound was consistent with what we experienced in the tunnel during the measurement process, and compared favorably to the sound produced by a first-order ambisonic decomposition of the B-format impulse response.

5   CONCLUSIONS

In this work we have presented measurements of the acoustic response of an excavated rock tunnel, and proposed a reverberation structure which can replicate these results. The reverberator could be applied in any situation in which the acoustic environment of a rock tunnel needs to be replicated. This could include game sound, film sound, and sound for simulators used for the training of machine operators. The reverberator is computationally efficient, and can additionally be applied in other applications where directional reverberation consisting of only diffuse sound is desired – for example as the late-reverberation portion of a more general reverberator. A more detailed description of the method is presented in [8].
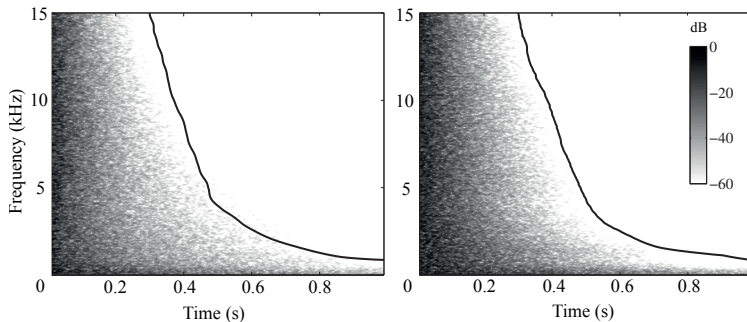
Figure 4: *Spectrorams and T_{60} estimates (solid line): measured impulse response (left), and modeled impulse response (right).*

6   ACKNOWLEDGMENTS

REFERENCES

[1] VÄLIMÄKI V, PARKER J D, SAVIOJA L, SMITH J O, & ABEL J S, Fifty years of artificial reverberation, *IEEE Trans. Audio, Speech, and Lang. Process.*, **20**(2012) 5, 1421–1448.

[2] JOT J M & CHAIGNE A, Digital delay networks for designing artificial reverberators, in *90th AES Conv.*, Paris, France, 1991.

[3] JOT J M, CERVEAU L, & WARUSFEL O, Analysis and synthesis of room reverberation based on a statistical time-frequency model, in *103rd AES Conv.*, New York, NY, USA, 1997.

[4] LEE K S, ABEL J S, VÄLIMÄKI V, STILSON T, & BERNERS D P, The switched convolution reverberator, *J. Audio Eng. Soc.*, **60**(2012) 4, 227–236.

[5] KARJALAINEN M & JÄRVELÄINEN H, Reverberation modeling using velvet noise, in *Proc. AES 30th Int. Conf.*, pages 1–9, Saariselkä, Finland, Mar. 2007.

[6] VÄLIMÄKI V, LEHTONEN H M, & TAKANEN M, A perceptual study on velvet noise and its variants at different pulse densities, *IEEE Trans. Audio, Speech, and Lang. Process.*, **21**(2013) 7, 1481–1488.

[7] PULKKI V, Virtual sound source positioning using vector base amplitude panning, *J. Audio Eng. Soc.*, **45**(1997) 6, 456–466.

[8] OKSANEN S, PARKER J, POLITIS A, & VÄLIMÄKI V, A directional diffuse reverberation model for excavated tunnels in rock, in *Proc. IEEE ICASSP 2013*, Vancouver, Canada, May 2013.

B   Publication II

S. Oksanen, J. Parker, and V. Välimäki, "Vibroacoustic Analysis and Synthesis of Struck Metal Bars Using Musical Instrument Modeling Techniques", in *Proc. of the Akustiikkapäivät 2013*, May 22–23, 2013, Turku, Finland.

VIBROACOUSTIC ANALYSIS AND SYNTHESIS OF STRUCK METAL BARS USING MUSICAL INSTRUMENT MODELING TECHNIQUES

Sami Oksanen, Julian Parker, and Vesa Välimäki

Aalto University, School of Electrical Engineering
Department of Signal Processing and Acoustics
P.O. Box 13000, FI-00076 AALTO, Espoo, Finland
sami.oksanen@aalto.fi, julian.parker@aalto.fi, vesa.valimaki@aalto.fi

Abstract

The objective for this research is to gain understanding of the sound generation of various bar geometries and impact types. First, the object under investigation was struck using a controllable and repetitive excitation method. The vibration properties of the bar, both longitudinal and transversal, were then measured using both strain gauges and microphones. The recorded signals were analyzed in the frequency-domain to find out which spectral components contributed to the sound generation of the bar. Measurements were carried out at the anechoic chamber of Department of Signal Processing and Acoustics in Aalto University. A computational model was developed based on the measured data. This model can be used to simulate vibration and sound generation on a specific point of the modeled bar. The computational model was constructed using current knowledge on physical modeling of musical instruments, utilizing techniques such as digital waveguides and allpass filters. The results of this study can be generalized and can be used in design and virtual prototyping of tools/working machines that generate transversal vibrations such as rock drills, hand-held machines, jack hammers, pile drivers.

1 INTRODUCTION

There are plenty of applications where impact energy is transmitted along steel bars to a surface to be impacted such as rock drilling equipment, breaking hammer tools, pile drivers, smaller hand held. As steel bars are suitable transmission lines for longitudinal power waves, a major side effect exists, the noise. Striking a metal bar with a metal object is known to be inherently noisy process. Typically a majority of the sound output is generated by the steel bar that is used to transmit the energy of piston impacts as compressive pulses along the steel bar to the desired object. The majority of the sound output is caused by the transversal vibrations that are generated as an unwanted side product of the main process. The non-parallel impacts are causing the generation of the transversal vibrations[1, 2]. Steel bar vibrations are divided to three categories based on the nature of the wave propagation, namely longitudinal, transversal, and torsional [3]. The amount of transversal vibrations with respect to longitudinal is dependent on various phenomena in the process [1]. Typically transversal vibrations are excited by non-parallel impacts [4]. Torsional vibrations propagate at extremely high frequencies (in the MHz range), and are not generally involved in audible sound output [5].

As the noise regulations are getting stricter and as the general awareness of noise reduction as an increased work environment safety procedure is increasing, there is a demand for deeper understanding of the vibration phenomena in such equipment. The gained understanding of the vibration properties of the steel bars can be used in various instances in noise reduction process.

This study presents an analysis of the steel bar vibration and based on the results a vibration model is constructed. Using such model can be beneficial in design and early prototyping of less noisy machinery parts. Results of the study can be exploited in design process of machine parts that are producing transversal vibrations.

This paper is organized as follows, first the basics of the steel bar vibrations is presented in Section 2. Then, measurements that were conducted during vibroacoustic analysis presented in Section 3. Next, a model for stress wave modeling is presented in Section 4. Finally conclusions are drawn in Section 5.

2   WAVE SPEED AND MODAL FREQUENCIES FOR STEELS BARS

The following formulation follows the presentation in [2]. The longitudinal wave speed C_{L} in a material is determined by the material dependent parameters Young's modulus E and material density ρ

$$C_{\mathrm{L}} = \sqrt{E/\rho}. \tag{1}$$

The frequency dependent transversal wave speed C_{T} can be formulated

$$C_{\mathrm{T}} = \sqrt{(\pi/2)(df_b C_{\mathrm{L}})}, \tag{2}$$

where d is the steel bar diameter, f_b is the transversal wave frequency. The longitudinal modal frequencies for a steel bar length of L_{r} is given by

$$f_{Ln} = \frac{nC_L}{2L_r}, \tag{3}$$

where n is the mode index. Modal frequencies of the transversal vibrations in a steel bar can be found frequencies where the steel bar length L_r is a half of the wavelength. The transversal modal frequencies of a steel bar can be determined based on the physical dimensions by

$$f_{Bn} = \frac{n^2\pi dC_L}{8L_r^2}\left[1 - 1.2\left(\frac{nd}{L_r}\right)^2\right]\left(\frac{2n+1}{2n}\right)^2. \tag{4}$$

The middle correction term (inside square brackets) is the correction term to take into account the rotary inertia and the shear force using the Timoshenko beam theory. The Timoshenko correction factor should be applied when $nD/L_r < 0.4$ .The last term of the Equation is the steel bar end condition correction factor for free-free (F–F) end conditions.
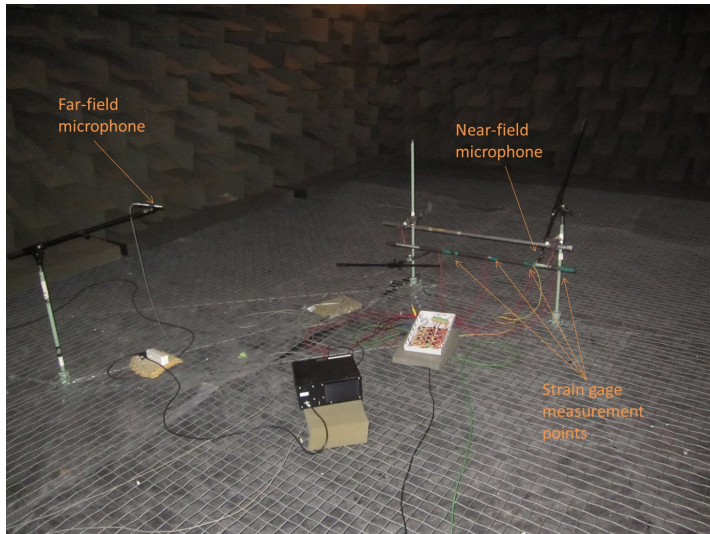
Figure 1: *Overall view of the measurement setup placed inside the anechoic chamber. The steel bar under investigation is rigged to the mounting frame. The audio signals are captured using near- and far-field microphones.*

3   VIBROACOUSTIC MEASUREMENTS

3.1   Acoustical Measurements

Acoustical measurements were carried out simultaneously with the strain wave measurements. The microphones were placed in the proximity of the excited objects (See Fig. 1). Measurement equipment consisted of B&K 4191 microphones, B&K 2669 pre-amplifiers and B&K Nexus 2690 microphone condition amplifier. The audio measurement equipment was connected to a RME FireFace 400 audio interface.

3.2   Strain and Stress Wave Measurements

A strain gage is a resistive component which is tightly attached to the surface of the object under investigation. When the object is exposed to compressive or tensile loading the strain gage resistance will change slightly based on the gage length variation. The change in resistance can then be monitored with a Wheatstone bridge circuit and a signal conditioning amplifier.
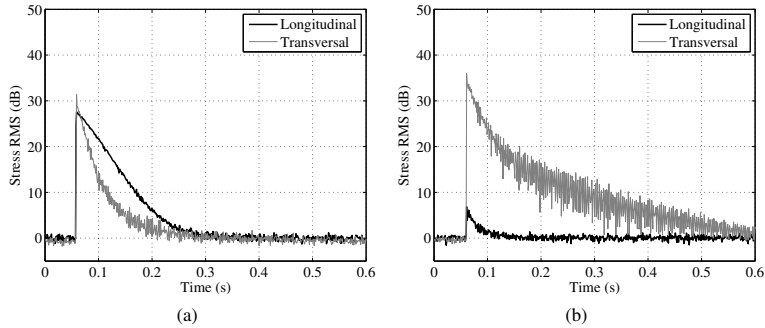
Figure 2: *RMS value as a function of time of the measured steel bar strain gage signals. Background noise level is normalized to 0 dB level. (a) Longitudinal impact (b) Transversal impact.*

3.3   Measurement Procedure

Measurements were conducted at the Department of Signal Processing and Acoustics. The large anechoic chamber was used during the measurements. The overall view of the measurement arrangements is presented in Figure 1 where a steel bar is being measured. The steel bar is attached to a custom-made holder which consists of aluminium tubes filled with insulation foam to damp the structure vibrations. The bar holder is attached to the permanently installed vertical poles inside the anechoic chamber. The steel bar in mounted on the holder at two points using thread and neoprene dampers. Neoprene dampers are used to isolate vibration transmission between the steel bar and the holder.

The steel bar was excited by hitting it at the end with a hand-held impact device. The excitation signal is only repeatable to some extent. More reliable results could be achieved using a device which could produce more repeatable impacts.

3.4   Measurement Results

The measured envelopes for longitudinal and transversal vibrations for a longitudinal impact is presented in Figure 2(a) and for transversal impact in Figure 2(b). The longitudinal vibrations are decaying linearly and transversal vibrations exponentially. An example of measured strain waves is presented in Figure 3(a). The upper plot shows the longitudinal strain waves. The shape of the longitudinal strain waves stays a rather constant as the waves reflect back and forth from the steel bar ends. The shape of the transversal strain wave has a very dispersive characteristic, and therefore a clear pulse cannot be distinguished from the response. The wave shape is caused by a frequency dependent wave speed that is slower at the low frequencies compared to the high frequency content.

The measured signal spectrums are presented in Figure 3(b). The spectrum of the longitudinal stress waves (top) has a harmonic distribution of the modal components. The transversal spectrum (middle) has an inharmonic distribution of the modal components that is caused by the dispersive wave propagation. The spectrum of the
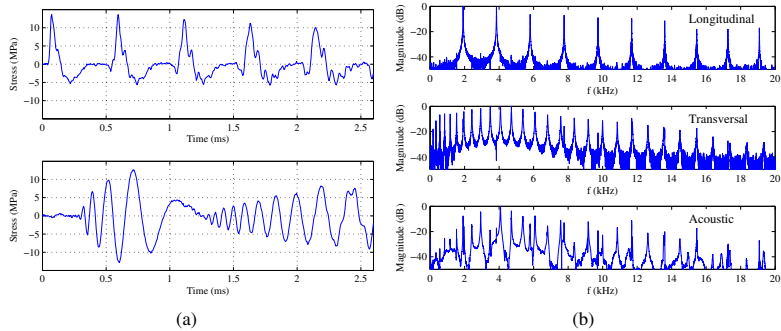
Figure 3: *Measured stress waves for steel bar exited with a longitudinal impact (a) Time-domain: longitudinal wave in the top plot and transversal wave in the bottom plot (b) Spectral-domain: longitudinal wave spectrum in the top plot, transversal wave spectrum in the middle plot and acoustic spectrum in the bottom plot.*

audio signal is a combination of the longitudinal and transversal modes. The spectral envelope of the audio signal has less energy at low frequencies ($f < 2$ kHz) than at higher frequencies. This is caused by the inefficient sound radiation of the steel bar at low frequencies.

4   MODELING OF STRESS WAVES IN A STEEL BAR

The modeling approach is divided into two domains, longitudinal and transversal. The strain wave models are implemented using digital waveguides. The digital waveguides have been previously used in the musical instrument modeling [6, 7]. A digital waveguide is a comb filter that is used to create spectral peaks to desired frequencies. The longitudinal model is a feedback comb filter with an adjustable delay line and reflection coefficient. The delay line length is used to tune the model to match desired spectral peaks. The reflection coefficient is used to adjust the signal decay rate.

The transversal model has a similar structure as the longitudinal model. The only difference is the dispersion filter in the feedback loop that is used to model the dispersion by mimicking the frequency dependent wave speed. The dispersion filter can be realized with allpass filters that are used to realize the desired phase delay characteristics. Finally the model is completed by summing up the modeled longitudinal and transversal vibrations.

5   CONCLUSIONS

A vibroacoustic analysis and synthesis of a struck metal bar was investigated in this paper. First the basics of the struck steel bar vibration were presented. The strain waves and related audio signals of the struck steel bar were measured in anechoic
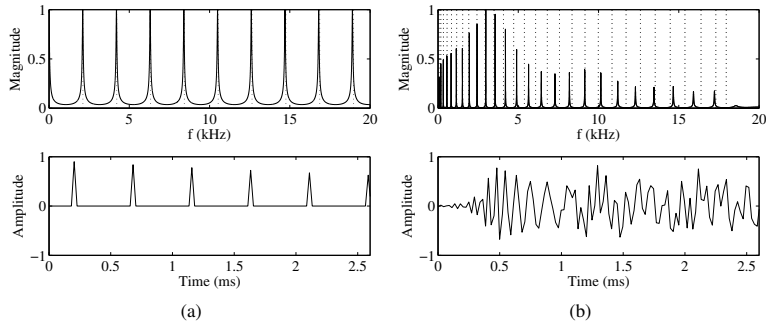
Figure 4: *Model output and spectrum (a) longitudinal and (b) transversal.*

conditions. Based on the measurements and vibration theory a computational model was developed using modeling techniques that have been already applied in the field of musical instrument modeling.

ACKNOWLEDGMENTS

REFERENCES

[1] CARLVIK I, The generation of bending vibrations in drill rods, *International Journal of Rock Mechanics and Mining Sciences & Geomechanics Abstracts*, **18**(1981) 2, 167–172.

[2] HAWKES I & BURKS J, Investigation of noise and vibration in percussive drill rods, *International Journal of Rock Mechanics and Mining Sciences & Geomechanics Abstracts*, **16**(1979) 6, 363–376.

[3] GRAFF K F, *Wave Motion in Elastic Solids*, Dover books on engineering, Dover Publications, 1975, reprint 1991.

[4] EREM'YANTS V & SLEPNEV A, Strain waves in colliding bars having nonparallel faces, *Journal of Mining Science*, **42**(2006) 6, 587–591.

[5] BILBAO S, *Numerical Sound Synthesis: Finite Difference Schemes and Simulation in Musical Acoustics*, John Wiley & Sons, 2009.

[6] SMITH J O, Physical modeling using digital waveguides, *Computer Music Journal*, **16**(1992) 4, 74–91.

[7] VÄLIMÄKI V, PAKARINEN J, ERKUT C, & KARJALAINEN M, Discrete-time modelling of musical instruments, *Reports on Progress in Physics*, **69**(2006) 1, 1–78.

C   Publication III

S. Oksanen, J. Parker, A. Politis, and V. Välimäki, "A directional diffuse reverberation model for excavated tunnels in rock", in *Proc. IEEE international Conference on Acoustics, Speech and Signal Processing ICASSP 2013*, May 26–31, 2013, Vancouver, Canada.

A DIRECTIONAL DIFFUSE REVERBERATION MODEL FOR EXCAVATED TUNNELS IN ROCK

Sami Oksanen, Julian Parker, Archontis Politis, and Vesa Välimäki

Aalto Univ., School of Electrical Engineering
Department of Signal Processing and Acoustics
P.O. Box 13000, FI-00076 AALTO, Espoo, Finland

ABSTRACT

Acoustic impulse responses of an excavated tunnel were measured. Analysis of the impulse responses shows that they are very diffuse from the start. A reverberator suitable for reproducing this type of response is proposed. The input signal is first comb-filtered and then convolved with a sparse noise sequence of the same length as the filter's delay line. An IIR loop filter inside the comb filter determines the decay rate of the response and is derived from the Yule-Walker approximation of the measured frequency-dependent reverberation time. The particular sparse noise sequence proposed in this work combines three velvet noise sequences, two of which have time-varying weights. To simulate the directional soundfield in a tunnel, the use of multiple such reverberators, each associated with a virtual source distributed evenly around the listener, is suggested. The proposed tunnel acoustics simulation can be employed in gaming, in film sound, or in working machine simulators.

Index Terms—Acoustic measurements, acoustic signal processing, convolution, reverberation

1. INTRODUCTION

Recorded impulse responses of spaces have been directly used as a means to add natural reverberation of a specific character to a dry recording, or as a way to listen how a specific space would affect a source signal, a process that in the context of architectural and virtual acoustics is termed auralisation [1, 2]. A straightforward way to achieve that is to convolve a source signal with a recorded room impulse response (RIR), which herein is termed as convolution reverberation [1]. An alternative approach, which provides more flexibility and computational efficiency, is to estimate the most relevant parameters from a recorded RIR and then map these parameters to common reverberation algorithms, such as combinations of delay-lines and feedback delay networks [3, 4, 5, 1]. Common parameters are mixing times between the early and late reverberant part, arrival times and amplitudes of discrete early reflections and reverberation times of the late diffuse part [6].

Fig. 1. Overall view of the main practice drilling tunnel. The sound source was located at the far end of the tunnel and receiver locations varied along the tunnel.

For surrounding multichannel rendering of reverberation, its directional characteristics should be taken into account, including direction of incidence of early echoes and overall directional distribution of energy and decay times of the late reverberant part [7]. A direct approach to generate multichannel RIRs for convolution reverberation from a directional recording is the ambisonic method [8], [9], in which a 4-channel B-format RIR is distributed to a multichannel loudspeaker setup by means of a least-squares inversion. For an overall description on the ambisonic methods and the B-format see [10]. However, due to the very limited angular resolution of first-order ambisonics, inter-channel coherence is high resulting in strong coloration of the reproduced reverberation in reproduction, position-dependent comb filtering effects and a reduced sense of diffusion.

A more recent method which utilizes the information encoded in the B-format in a more perceptually-relevant way is the Spatial Impulse Response Rendering (SIRR) [11]. SIRR performs a time-frequency energetic analysis on the B-format RIR and decomposes it in a directional part, which contains the direct sound and strong reflections, panned to the appropriate speakers by means of vector-base amplitude panning (VBAP) [12], and a diffuse part which is reproduced by all loudspeakers by means of decorrelating filters. Another recent approach similar in spirit to SIRR, but for arbitrarily spaced arrays instead of B-format input, is the one presented in [13]. Both of these methods achieve high-quality rendering of recorded responses, however the end product is meant for convolution reverberators, mainly for auralisation of concert halls. In addition, the

time-frequency analysis and synthesis of the RIRs can be computationally intensive for many applications.

This work's relation to prior research is that the use of artificial reverberation is expanded from concert halls and rooms to tunnels, and a novel directional reverberation algorithm is introduced. This study presents an efficient algorithm for surrounding reverberation also based on a B-format RIR, which avoids the computational load of convolution reverbs while retaining the basic directional characteristics of the reverberation. The algorithm is suitable for diffusive spaces without dominant reflections, such as the cave space under study, or as a processing block in a system that handles the early reflections separately. Prior work of modeling tunnel reverbs includes the study by Collecchia et al. [14] where a method to model tunnel systems using digital waveguide networks is presented. However, it does not cover directional reverberation modeling.

In Sec. 2, we describe the measurement of the B-Format impulse response of an excavated rock tunnel, and present some analysis of its main characteristics. In Sec. 3 we present a method of approximating this reverberation for arbitrary input through a novel multichannel sound reproduction system. In Sec. 4, we conclude.

2. TUNNEL IMPULSE RESPONSE MEASUREMENTS

The measured space is a teaching and test tunnel located at the Aalto University campus, see Fig. 1. The characteristics of the tunnel match closely the ones at excavation and underground construction sites. The tunnel floor consists of a layer of gravel on top of the bedrock. Parts of the tunnel walls and ceiling are reinforced with sprayed plaster coating, but the majority of the wall area is bare and extremely uneven rock.

The acoustic properties of the space were determined using the standard log-sweep method [15, 16]. A sound source is located at a certain position within the tunnel, and a set of logarithmic sine sweeps are played. The acoustic response to this sweep is measured using a microphone positioned at a pre-determined location, at a great enough distance to be well within the reverberant soundfield. Sound signal playback and recording were carried out with custom made software in Matlab. Log-sweep duration was 10 s and frequency range was 20 Hz to 20 kHz. The excitation signal was repeated five times in each speaker and receiver position to help avoid sources of random error.

The excitation signals were produced using a stand-mounted active loudspeaker (Genelec 1032A). To approximate an omnipolar acoustic excitation with the directional speaker, the measurements were conducted in seven different speaker orientations and averaged. The set of speaker orientations consisted of six positions in the horizontal plane 60 degrees apart from each other and one where loudspeaker was pointing upwards. The response measurements were also carried out using a passive omnipolar loudspeaker. The omnipolar loudspeaker was limited in efficiency and was not capable of producing the high SPLs required at greater distances, so the omnipolar measurements were used to verify the results produced by the directional speaker.

Acoustic responses were measured using a pressure-field microphone (B&K 4192) and a B-format Soundfield microphone (ST 350) simultaneously. The microphones were placed approximately 1.5 m above the floor and close to the axial line of the tunnel. The distance between microphones was approximately 30 cm. The distance of the receiver point from the sound source was varied from 5 m to 20 m.
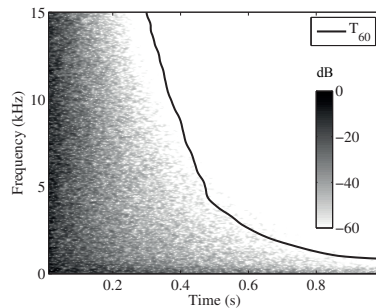

Fig. 2. Spectrogram of the measured impulse response and estimated T_{60} value.

The impulse response of the space is derived from the measured responses by convolving it with the time reversed version of the excitation signal. The impulse responses are then time-aligned and averaged with the other appropriate measurements. In the case of the directional speaker, this is all repeated for measurements at the seven different angles for a particular distance between sound source and receiver. In the omnipolar speaker case, this is just the repeated measurements made at that distance.

2.1. Analysis of measured responses

The first step of analysis was to compare the responses produced by the average of directional speaker responses with those produced by the omnidirectional speaker. The results produced agree closely enough to suggest that the average of directional speaker responses is a good approximation, especially within the horizontal plane. The omnidirectional speaker has a poor response below around 100 Hz, and so verification is not possible below that frequency. However, at this frequency the directionality of the Genelec 1032A is less pronounced, so we assume that the approximation holds.

Figure 2 shows a spectrogram of the response produced using the average of directional speaker responses, taken at a distance of 13m between source and receiver. The response is created from the B-format signal recorded at the Soundfield microphone by creating a virtual microphone pointing towards the source. Overlayed on the spectrogram is the estimated T_{60} with respect to frequency. Inspection of the spectrogram shows that the response consists of only diffuse sound, with no clear discrete echoes visible.

Figure 3 shows relative T_{60} times of the responses produced by calculating eight different virtual microphones from the B-format signal, pointing in eight directions distributed evenly around the circle. It should be clear from inspection that there is a fairly significant variation of frequency dependent reverberation time with direction.

3. A DIRECTIONAL DIFFUSE REVERBERATION MODEL

As can be seen in the analysis of the measured responses of the tunnel given above in Sec. 2, the defining characteristic of reverberation in an irregular rock tunnel is that no strong early reflections are
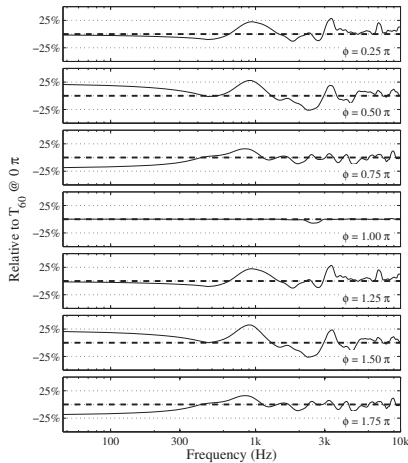
Fig. 3. Relative difference in T_{60} with respect to direction ϕ.

present, only a diffuse tail. The density of echoes is also extremely high from the start of the response. The response is similar to that of a plate reverberator in these respects [17, 18, 19]. The other interesting aspect of the measured reverberation is the frequency-dependent variation of T_{60} with angle. A successful model should be able to reproduce this fast onset of diffuse sound, as well as being computationally efficient enough to be used in multi-channel or spatial audio context to reproduce the directional nature of the sound field.

The first task in the production of the model was to choose an appropriate modeling approach. Physical modeling of the space via FDTD or some form of acoustic ray-tracing is not ideal, due to the complex irregular geometry of the tunnel's rock walls. Convolution with a measured impulse response is an option, but is inflexible and computationally inefficient if we want to produce a model which accurately reproduces the frequency dependent T_{60} in multiple directions. Traditional algorithmic reverberation methods of the Schroeder [20], Moorer [21] or Gardner [22] type have difficulty producing the immediate onset of dense echoes necessary [1]. A Feedback Delay Network (FDN) [3] is reasonably appropriate, although again there can be difficulty in easily producing the immediate density of reflections necessary. The most appropriate solution would appear to be one based on convolution with a sparse noise sequence [23, 24]. This method has been shown to be more computationally efficient than a comparable FDN [24], and by its nature is entirely diffuse for the whole duration.

3.1. Single-channel reverberation structure

The basic reverberation structure is similar to those presented by Lee et al. [24], with some modifications. The core idea of the approach is that the diffuse tail of an acoustic response can be approximated by convolution with exponentially decaying white noise. However, direct convolution with exponentially decaying white noise has some
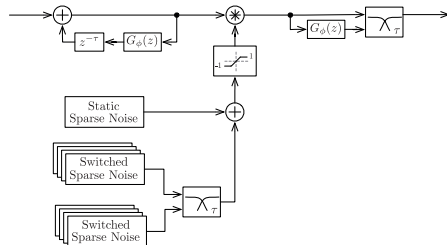

Fig. 4. Block diagram showing structure of a single channel of the novel reverberator.

drawbacks – namely that it is inefficient and lacks the possibility of varying reverberation time with frequency. Instead, we can use a comb filter to produce a series of exponentially decaying repeats of the input signal, and then convolve with a shorter sequence of noise to fill the gaps. The result is very close to the direct convolution, but computationally much less expensive. Frequency dependent reverberation time can be obtained by the addition of a damping filter into the feedback loop of the comb filter.

The efficiency of such a structure can be improved further by utilizing a form of sparse noise (noise that contains many zeros) instead of Gaussian white noise. Karjalainen and Järveläinen [23] propose one such type of noise, which they call 'velvet noise'. This particular sparse noise possesses the desirable quality of a constant, non-lumpy distribution in time. This quality manifests itself as an audible smoothness. This density of this form of noise may be greatly reduced (down to as low as several thousand impulses per second) whilst still being audibly equivalent to Gaussian noise [23, 25].

The disadvantage of this approach to reverberation is that depending on the exact structure of the reverberator, unwanted artifacts may be produced for certain types of signal. For example, if a static noise sequence is calculated once and used constantly, a periodic element is clearly audible in the response of the system to transients [23, 24]. Conversely, this periodicity is hidden during the systems response to steady-state signals, which contain no audible artifacts. To mitigate this periodicity it is necessary to vary the sparse noise sequence over time. The most basic form of this variation is to replace the noise sequence each time one cycle through the comb-filter has been completed. This modification removes the periodicity from the response to transient signals completely, but when a steady-state signal is applied heavy modulation of the sound is audible. Therefore, much of the difficulty in designing this type of reverberator is to find the correct form and type of variation of the noise sequence which strikes a balance between audible periodicity and unwanted modulation, and ideally makes both of these artifacts inaudible. Lee et al. [24] suggest several such types of variation. The method used in this work is a new hybrid of these methods, with some extension.

The other major challenge of this form of reverberation is modifying the sparse noise sequence so that continuity is maintained between the sections delineated by the echoes of the comb-filter. In the case of frequency-independent reverberation time, this is simply a case of providing the noise sequence with an exponentially decaying envelope dependent on the length and damping coefficient
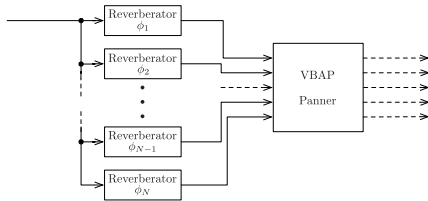
Fig. 5. Block diagram showing structure of complete multi-channel reverberator.

Fig. 6. Spectrogram of the impulse response of the novel reverberator and its T_{60} estimate. Compare with Fig. 2.

of the comb filter. In the case of frequency-dependent reverberation-time, Lee et al. [24] suggest crossfading between an unfiltered noise-sequence and the same noise sequence filtered with the damping filter.

Figure 4 shows the proposed structure of the reverberator. It consists of a comb filter of length τ samples, containing a damping filter $G_\phi(z)$. This damping filter is an IIR filter derived from Yule-Walker approximation of the frequency-dependent T_{60} of the measured tunnel response for a particular direction. The output of this comb filter is convolved with a sparse noise sequence of length τ. This sparse noise sequence is a new hybrid of the non-overlapping sequence and overlapping sequence methods described by Lee et al. [24]. Three noise sequences are generated. Firstly, a static noise sequence of low density (500 impulses per second). Secondly, two denser noise sequences (2000 impulses per second) are generated, and crossfading is performed between them over each comb-filter period τ. At the end of a comb-filter period, the first noise-sequence (where the crossfading started) is replaced by the second noise sequence, which is then in turn replaced by a newly generated noise sequence. This process repeats for every comb-filter period τ. The crossfaded noise sequence is added to the static noise sequence, passed through a hard clipper to remove the occasional occurrences of co-incident (and hence double amplitude) impulses, and then convolved with the output of the comb-filter. This combination of static and varying sparse noise was chosen as it successfully suppressed artifacts whilst still being sparse enough to keep the convolution efficient. Finally, the convolved signal is crossfaded over each period τ with a version of itself filtered by the damping filter $G_\phi(z)$, in order to approximate the correct envelope. Experimentation showed that best results were obtained when the comb-filter period is $\tau \approx 30$ ms.

3.2. Extending the model for directional reverberation

To extend the reverberation structure to a directional model, we make the assumption that due to the highly diffuse nature of the reflections, the sound arriving from different directions is essentially uncorrelated. We can then approximate the directional response by the use of a number of separate reverberators, each of which is treated as a virtual source within the space, and spatialized according to some established system for distribution to a loudspeaker system. In this case, we use VBAP [12] to perform this spatialization. For headphone audio applications, a spatialization scheme making use of HRTFs could replace VBAP. Each reverberator ϕ_n has its damping filter G_{ϕ_n} derived from the directional T_{60} time measured in the same direction as the corresponding virtual source. For the pur-
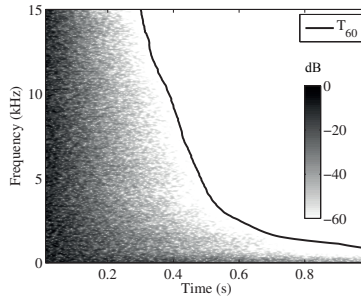
pose of this work we employed 8 reverberators and hence 8 virtual sources, distributed evenly at increments of $\frac{\pi}{4}$ in a plane around the listener. The dry signal is also treated as a virtual source, and placed at the front of the space, to be consistent with the position of the source during the measurements. It is possible that a smaller number of virtual sources and reverberators could be used without much loss of directional information due to the limited angular resolution of the B-Format microphone. Figure 5 shows this structure.

3.3. Results

Figure 6 shows spectrogram of the impulse response of the first reverberator (and hence first virtual source) in the model described above. The first reverberator is placed at zero angle (i.e. straight ahead). This response can be compared to the measured response given in Figure 2, which is the response to which the frequency dependent reverberation of this particular reverberator has been fitted. The diffuse nature of the reverberation seems to have been captured correctly, and the T_{60} is approximated well.

The model was tested with a variety of input sounds, on an 8.1 surround audio system in a listening room conforming to the ITU-R BS.1116 standard. The resulting sound was consistent with what we experienced in the tunnel during the measurement process, and compared favorably to the sound produced by a first-order ambisonic decomposition of the B-format impulse response. Sound samples are available for download.[1]

4. CONCLUSIONS

In this work we have presented measurements of the acoustic response of an excavated rock tunnel, and proposed a reverberation structure which can replicate these results. The reverberator could be applied in any situation in which the acoustic environment of a rock tunnel needs to be replicated. This could include game sound, film sound, and sound for simulators used for the training of machine operators. The reverberator is computationally efficient, and can additionally be applied in other applications where directional reverberation consisting of only diffuse sound is desired – for example as the late-reverberation portion of a more general reverberator.

---

[1] http://www.acoustics.hut.fi/go/icassp13-caverev/

5. REFERENCES

[1] V. Välimäki, J. D. Parker, L. Savioja, J. O. Smith, and J. S. Abel, "Fifty years of artificial reverberation," *IEEE Transactions on Audio, Speech, and Language Processing*, vol. 20, no. 5, pp. 1421–1448, Jul. 2012.

[2] M. Vorländer, *Auralization: Fundamentals of Acoustics, Modelling, Simulation, Algorithms and Acoustic Virtual Reality*, Springer London, London, UK, 2008.

[3] J.-M. Jot and A. Chaigne, "Digital delay networks for designing artificial reverberators," in *90th AES Convention*, Paris, France, 1991.

[4] R. Stewart and D. Murphy, "A hybrid artificial reverberation algorithm," in *122nd AES Convention*, Vienna, Austria, 2007.

[5] A. Primavera, S. Cecchi, L. Romoli, P. Peretti, and F. Piazza, "An advanced implementation of a digital artificial reverberator," in *130th AES Convention*, London, UK, 2011.

[6] J.-M. Jot, L. Cerveau, and O. Warusfel, "Analysis and synthesis of room reverberation based on a statistical time-frequency model," in *103rd AES Convention*, New York, NY, USA, 1997.

[7] M. Kuster, "Multichannel room impulse response rendering on the basis of underdetermined data," *Journal of the Audio Engineering Society*, vol. 57, no. 6, pp. 403–412, June 2009.

[8] M. A. Gerzon, "Recording concert hall acoustics for posterity," *Journal of the Audio Engineering Society*, vol. 23, no. 7, pp. 569–571, 1975.

[9] A. Farina and R. Ayalon, "Recording concert hall acoustics for posterity," in *Proc. 24th International Conference of AES: Multichannel Audio, The New Reality*, Banff, Alberta, Canada, 2003.

[10] M. A. Gerzon, "Ambisonics in multichannel broadcasting and video," *Journal of the Audio Engineering Society*, vol. 33, no. 11, pp. 859–871, 1985.

[11] J. Merimaa and V. Pulkki, "Spatial impulse response rendering I: Analysis and synthesis," *Journal of the Audio Engineering Society*, vol. 53, no. 12, pp. 1115–1127, 2005.

[12] V. Pulkki, "Virtual sound source positioning using vector base amplitude panning," *Journal of the Audio Engineering Society*, vol. 45, no. 6, pp. 456–466, Jun. 1997.

[13] S. Tervo, J. Pätynen, A. Kuusinen, and T. Lokki, "Spatial decomposition method for room impulse responses," *Journal of the Audio Engineering Society*, vol. 61, no. 1/2, pp. 16–27, 2013.

[14] R. E. Collecchia, M. A. Kolar, and J. S. Abel, "A computational acoustic model of the coupled interior architecture of ancient Chavín," in *133th AES Convention*, San Francisco, CA, USA, Oct. 2012.

[15] A. Farina, "Simultaneous measurement of impulse response and distortion with a swept-sine technique," in *108th AES Convention*, Paris, France, Feb. 2000.

[16] S. Müller and P. Massarani, "Transfer-function measurement with sweeps," *Journal of the Audio Engineering Society*, vol. 49, no. 6, pp. 443–471, 2001.

[17] K. Arcas and A. Chaigne, "On the quality of plate reverberation," *Applied Acoustics*, vol. 71, no. 2, pp. 147–156, 2010.

[18] S. Bilbao, K. Arcas, and A. Chaigne, "A physical model for plate reverberation," in *Proc. IEEE International Conference on Acoustics, Speech, and Signal Processing*, Toulouse, France, May 2006, vol. 5, pp. 165–168.

[19] S. Bilbao, "A digital plate reverberation algorithm," *Journal of the Audio Engineering Society*, vol. 55, no. 3, pp. 135–144, Mar. 2007.

[20] M. R. Schroeder, "Natural-sounding artificial reverberation," *Journal of the Audio Engineering Society*, vol. 10, no. 3, pp. 219–223, July 1962.

[21] J. Moorer, "About this reverberation business," *Computer Music Journal*, vol. 3, no. 2, pp. 13–28, 1979.

[22] W. Gardner, "A realtime multichannel room simulator," in *Proc. 124th meeting of the Acoustical Society of America*, New Orleans, LA, USA, Nov. 1992.

[23] M. Karjalainen and H. Järveläinen, "Reverberation modeling using velvet noise," in *Proc. 30th International Conference of AES: Intelligent Audio Environments*, Saariselkä, Finland, Mar. 2007, pp. 1–9.

[24] K. S. Lee, J. S. Abel, V. Välimäki, T. Stilson, and D. P. Berners, "The switched convolution reverberator," *Journal of the Audio Engineering Society*, vol. 60, no. 4, pp. 227–236, Apr. 2012.

[25] V. Välimäki, H.-M. Lehtonen, and M. Takanen, "A perceptual study on velvet noise and its variants at different pulse densities," *IEEE Transactions on Audio, Speech, and Language Processing*, vol. 21, 2013.

D   Publication IV

S. Oksanen, J. Parker, and V. Välimäki. "Physically informed synthesis of jackhammer tool impact sounds", in *Proc of the 16th International Conference on Digital Audio Effects DAFx-13*, Sept. 2–6, 2013, Maynooth, Ireland.

PHYSICALLY INFORMED SYNTHESIS OF JACKHAMMER TOOL IMPACT SOUNDS

Sami Oksanen, Julian Parker, and Vesa Välimäki

Department of Signal Processing and Acoustics
Aalto University, Espoo, Finland
`sami.oksanen@aalto.fi`

ABSTRACT

This paper introduces a sound synthesis method for jackhammer tool impact sounds. The model is based on parallel waveguide models for longitudinal and transversal vibrations. The longitudinal sounds are produced using a comb filter that is tuned to match the longitudinal resonances of a steel bar. The dispersive transversal vibrations are produced using a comb filter which has a cascade of first-order allpass filters and time-varying feedback coefficient. The synthesis model is driven by an input generator unit that produces a train of Hann pulses at predetermined time-intervals. Each pulse has its amplitude modified slightly by a random process. For increased realism each impact is followed by a number of repetitive impacts with variable amplitude and time difference according to the initial pulse. The sound output of the model is realized by mixing both transversal and longitudinal signals and the effect is finalized by an equalizer.

1. INTRODUCTION

The jackhammer sound is a familiar part of the soundscape of the city, being commonly used in both road works and on building sites. A simulation of this sound would be a useful part of the repertoire for sound designers working with audio for games or film.

The sound generation in rock or concrete breaking is caused by the main functional parts of the rock breaking device, including the power generating unit, the breaking tool, and the pneumatic devices exhaust air from the muffler [1, 2]. Typically the majority of the sound output is generated by the mechanism that is used to transmit the piston impacts as compressive pulses along the tool to the rock. The compressive pulses excite the breaking tool vibrations [3, 2, 4]. Steel bar vibrations are divided to three categories based on the nature of the wave propagation, namely longitudinal, transversal, and torsional [5]. The amount of transversal vibrations with respect to longitudinal is dependent on various phenomena [6]. Typically transversal vibrations are excited by non-parallel impacts [7]. Torsional vibrations propagate at extremely high frequencies (in the MHz range), and are not generally involved in audible sound output [8].

The approach in this paper is based in modeling the physical properties of musical instruments i.e. instruments with dispersive rigid bar vibration such as tubular bells [9, 10] or more general objects like springs which exhibit dispersive propagation [11, 12]. Digital waveguide techniques that are previously used in musical instrument modeling [13, 14] are now applied to tool sound synthesis. Some work on non-musical sound synthesis has been done e.g. in the field of automotive sound synthesis [15, 16], and various approaches by applying procedural audio methods to everyday sound sources [17], hand clapping [18], foot steps [19], and sounding objects [20]. However, the field of machine tool sound synthesis is fairly novel. Hoffmann et al. [21] modeled surgical drill sounds with a sinusoidal model.

The scope of this paper is to introduce a sound synthesis model for jackhammer impact sounds. The proposed model has multiple parameters to adjust the sound output in order to meet the nuances of different tool constructions, operational conditions and impact parameters.

This paper is organized as follows. First, the basics of tool vibrations are discussed in Sec. 2. Then, the proposed sound synthesis method is introduced and the main functional parts are explained in Sec. 3. Next, model results are presented and discussed in Sec. 4. Finally, conclusions are drawn in Sec. 5.

2. TOOL VIBRATIONS

A jackhammer tool is a solid steel bar with a round or hexagonal cross-section. The size of the tool varies according to size of the jackhammer machine. Typically the tool length can vary between 30 cm to nearly 1 m and diameter varies between 15 mm to 50 mm. The longitudinal modal frequencies for steel bar are determined by

$$f_{\mathrm{L}} = \frac{kc_{\mathrm{s}}}{2l}, \tag{1}$$

where k is the mode index, $c_{\mathrm{s}} = 5200$ m/s is the speed of sound in steel, and l is the bar length. Hawkes and Burks [1] presented the following definition for transversal modal frequencies

$$f_{\mathrm{T}} = \frac{k^2 \pi d c_{\mathrm{s}}}{8l^2} \left[1 - 1.2 \left(\frac{kd}{l} \right)^2 \right] \left(\frac{2k+1}{2k} \right)^2, \tag{2}$$

where d is diameter of the bar. The middle term applies the Timoshenko correction at lower frequencies where modes are located at more dense intervals. The final term of the equation accounts for the boundary conditions of the bar.
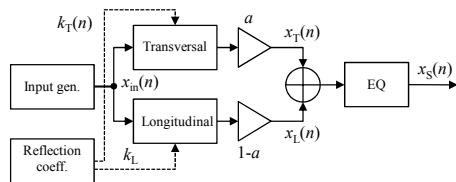

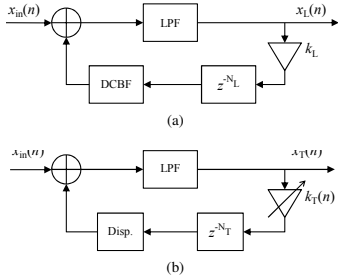Figure 1: *Jackhammer tool sound synthesis model.*

Figure 2: *Synthesis units, (a) longitudinal and (b) transversal.*

Figure 3: *Dispersion filter design, impulse responses of varying length M cascade of first-order allpass filters $\lambda = -0.618$ (top left) and with $\lambda = -0.918$ (top right). Phase delay curves for different cascade lengths with $\lambda = -0.618$ (bottom left) and $\lambda = -0.918$ (bottom right).*

3. PROPOSED MODEL

The proposed sound synthesis model is presented in Fig. 1. The model has five main functional units, namely input generator, longitudinal vibration unit, transversal vibration unit, reflection coefficient generator for transversal unit, and equalizer. The sound output $x_S(n)$ is a weighted sum of longitudinal $x_L(n)$ and transversal $x_T(n)$ output signals. The spectral balance of the model output is adjusted using an equalization filter (EQ) for summed longitudinal and transversal outputs. A first-order highpass filter (-6 dB @ 800 Hz) is used to equalize the model output to compensate for ineffective sound radiation at low frequencies. The functionality of each block is explained in more detail in the following sub-sections.

3.1. Longitudinal Vibration Model

The longitudinal vibration model is based on a digital comb filter with a lowpass filter (LPF) in the feed-forward section and a delay line in feedback loop (see Fig. 2a). The longitudinal model is tuned to match the resonance frequencies (Eq. 1) of the tool by adjusting the delay line length N_L. The reflection coefficient k_L is used to adjust the desired decay time for the filter impulse response. To avoid the unwanted effects of a DC-bias in the model output, the longitudinal model has a DC-blocking filter (DCBF) [22] inside the feedback loop. The DC-blocking filter has the transfer function

$$H_{DCB}(z) = \frac{1 - z^{-1}}{1 - Rz^{-1}}, \qquad (3)$$

where R is used to set desired cutoff frequency, for longitudinal model $R = 0.995$ having the -6 dB point at about 20 Hz.

3.2. Transversal Vibration Model

The transversal vibration model is presented in Fig. 2b. It is based on a similar structure to the longitudinal model. The main difference between models is the dispersion filter (DISP) and the time-varying reflection coefficient $k_T(n)$ in the transversal model. The time-varying reflection coefficient is used to simulate the damping of vibration that occurs whilst the excitation mechanism is in contact with the tool.

Transversal vibrations in a steel bar are strongly dispersive [5]. The approach to modeling transversal vibrations begins with the dispersion filter design process. The dispersion is modeled using a
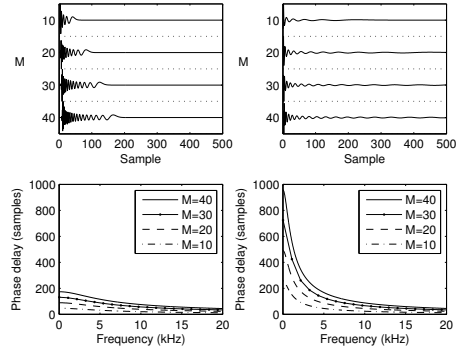
first-order allpass filter as a prototype. The first-order allpass filter transfer function is

$$H_{AP}(z) = \frac{\lambda + z^{-1}}{1 + \lambda z^{-1}}, \qquad (4)$$

where λ is used to adjust the filter group-delay response. In a steel bar, high-frequency transversal waves travel faster than low-frequency transversal waves, which implies that we should choose $\lambda < 0$. The amount of dispersion achieved using a single filter is not enough to match the dispersion characteristics of a steel bar. To increase the amount of dispersion in the model a cascade of first-order allpass filters [12, 23, 24] is used

$$H_{Cas}(z) = \left(\frac{\lambda + z^{-1}}{1 + \lambda z^{-1}} \right)^M, \qquad (5)$$

where M is the cascade length.

The effect of cascade length is presented in Fig. 3 (top left) where impulse responses of cascade lengths $M = 10 \ldots 40$ are presented. The lower subplot shows corresponding phase delays for filter cascades with $\lambda = -0.618$. For comparison, the effect of a change in λ value is presented in Fig. 3 (top right), where impulse responses of filters with the different cascade lengths are demonstrated with $\lambda = -0.918$.

3.3. Input Generation

The sound synthesis model is excited using input sequence vector $x_{in}(n)$ containing a series of Hann pulses spaced according to the desired impact rate. The width and spacing of input pulses can be adjusted. The input pulse width affects the model output spectrum according to input pulse spectral content, i.e. wider pulses will produce less high-frequency content. Based on informal evaluation, pulse widths from 7 to 11 samples (@ 44.1 kHz) were recognized to produce the most realistic sound output.
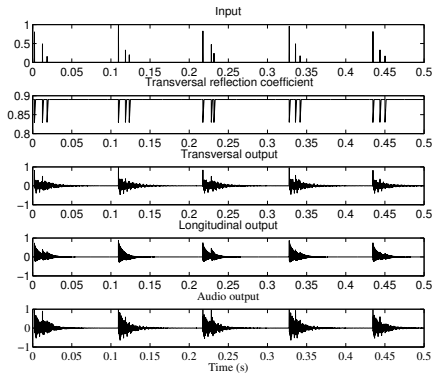
Figure 4: *Synthetic time-domain signals for series of impacts.*

Figure 5: *Synthetic time-domain signals for a single impact.*

The spacing between pulses can be set to meet the desired impact rate of the jackhammer under investigation. Typical impact rates of jackhammers can vary from 10 to 40 Hz. The amplitude of a single impact varies with each strike because of the varying state of the piston and tool. The tool could be in firm contact with the material being broken when the piston impact occurs, or there could be no contact at all.

Pulse repetitions are added to $x_{in}(n)$ after each main impact to model the bouncing of the tool which will happen after the initial impact. The number and amplitude of the repetitions can be adjusted. The succeeding impacts are randomly spaced after the initial impact with a time difference varying from 5–10 % of the main impulse time difference. The pulse repetitions have a randomly chosen decaying amplitude. An example of a five impact series with pulse repetitions is presented in Fig. 4 (bottom). The produced input sequence is used to drive both longitudinal and transversal models.

3.4. Time-Varying Reflection Coefficient for Transversal Model

The input dependent time-varying reflection coefficient vector k_T for the transversal model is generated based on the excitation vector $x_T(n)$. The reflection coefficient vector k_T is initialized to value k_{Tmax}. At the beginning of each excitation pulse a linear transition ramp is generated to modulate $k_T(n)$ value from k_{Tmax} to k_{Tmin} at a randomized slope ratio. After $k_T(n)$ has reached k_{Tmin} an increasing ramp is generated to resume $k_T(n)$ to k_{Tmax}. An example of k_T for single excitation pulse is presented in Fig. 5 (second from top).

4. RESULTS

The sound output produce by the model for single impact without pulse repetitions is presented in Fig. 5 (bottom). The input pulse length is nine samples (top), $k_{Tmin} = 0.83$, $k_{Tmin} = 0.89$, $k_L = 0.94$, $\lambda = -0.618$. Output from the transversal model (middle) has a dispersive nature, the initial pulse can be distinguished from the plot but succeeding pulses are smeared in time due to dispersion. The longitudinal model output (second from bottom)
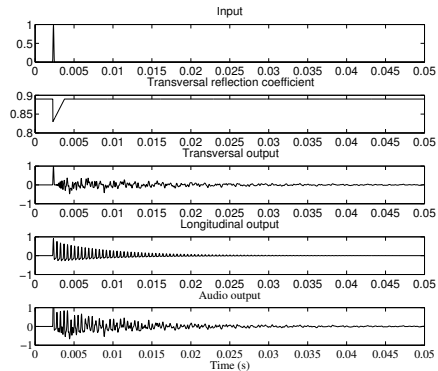
shows decaying pulse reflections, but the pulse shape of the input can still be recognized. The time-varying transversal reflection coefficient (second from top) shows the linear pulse decay in time.

Spectral plots are presented in Fig. 6. The upper subplot shows the spectrums of the longitudinal output and input signal. The transversal spectrum is presented in the middle subplot and the spectrum of the total sound output is presented in the bottom subplot. It can be seen that the spectrum of the input pulse shapes the spectral envelopes of the model outputs. Depending on the pulse duration and tool diameter there can be instances where individual modal components can vanish from the model output. For example, the mode in the longitudinal model output is seen at around 8.5 kHz in Fig. 6 (bottom).

The model output for a series of impacts in the time-domain is presented in Fig. 4 and in the spectral domain in Fig. 7. The impact rate is approxim. 10 Hz, each main impact is followed by fast repetitions at variable time intervals. The transversal reflection coefficient value is modulated by the impacts. When the repetitive impact arrives before the reflection coefficient has reached its upper threshold, k_{Tmax}, the reflection coefficient value is set to upper threshold k_{Tmax}. Examples of the audio produced by the model are available for download[1].

5. CONCLUSIONS

A sound synthesis model for impact sounds of a jackhammer tool was presented in this paper. The model is based on the physical vibration properties of a steel bar that is excited with a series of Hann pulses. The model consists of both a longitudinal and a transversal vibration model, an input and reflection coefficient generator unit, and an equalizer. The model has various control parameters that can be used to modify the sound output according to the sound synthesis goals. The model is intended to be used as part of a procedural sound environment generation system, for use in simulators or games.

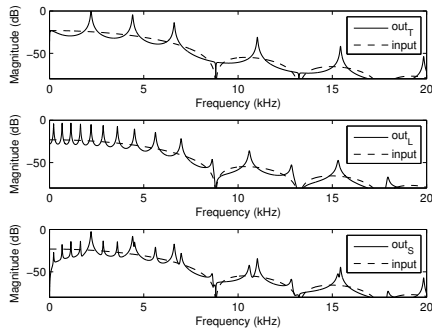[1]http://www.acoustics.hut.fi/go/dafx13-impact/

Figure 6: *Signal spectrum, longitudinal (top), transversal (middle), and summed output (bottom). The spectrum of the input pulse is plotted with dashed line.*
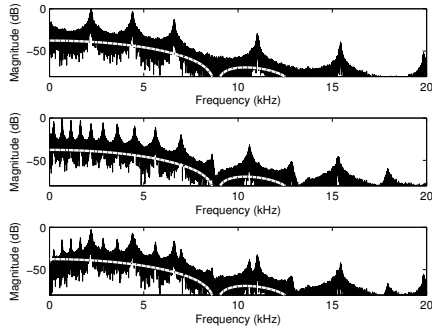

Figure 7: *Signal spectrum for series of impacts, longitudinal (top), transversal (middle), and summed output (bottom). The spectrum of the input pulse is plotted with dashed line.*

6. ACKNOWLEDGMENTS

7. REFERENCES

[1] I. Hawkes and J.A. Burks, "Investigation of noise and vibration in percussive drill rods," *Int. J. Rock Mech. and Mining Sci. & Geomech. Abstr.*, vol. 16, no. 6, pp. 363–376, 1979.

[2] J.-E. Ögren, *Noise Radiation from Drill Steels*, Ph.D. thesis, Luleå University of Technology, Luleå, Sweden, 1983.

[3] P. K. Dutta, J. A. Burks, and R. C. Bartholomae, "Measurement and analysis of the stress wave generated rod noise in percussive rock drill," in *Proc. SESA 1981 Spring Meeting*, Dearborn, MI, USA, 1981, pp. 218–226.

[4] A. Akay, M.T. Bengisu, and M. Latcha, "Transient acoustic radiation from impacted beam-like structures," *J. Sound and Vibration*, vol. 91, no. 1, pp. 135–145, 1983.

[5] K. F. Graff, *Wave Motion in Elastic Solids*, Dover books on engineering. Dover Publications, 1975, Reprint 1991.

[6] N. Dongmin, "Rigid impact – the mechanism of percussive rock drilling," in *Proc. 42nd US Rock Mech. Symp.*, San Francisco, CA, June 29th – July 2nd 2008, pp. 1–5.

[7] V.E. Erem'yants and A.A. Slepnev, "Strain waves in colliding bars having nonparallel faces," *Journal of Mining Science*, vol. 42, no. 6, pp. 587–591, 2006.

[8] S. Bilbao, *Numerical Sound Synthesis*, Wiley, 2009.

[9] N. H. Fletcher and T. D. Rossing, *The Physics of Musical Instruments*, Springer-Verlag, 1991.

[10] R. Rabenstein, T. Koch, and C. Popp, "Tubular bells: A physical and algorithmic model," *IEEE Trans. Audio, Speech, and Lang. Process.*, vol. 18, no. 4, pp. 881–890, 2010.

[11] J. Parker, H. Penttinen, S. Bilbao, and J. Abel, "Modeling methods for the highly dispersive Slinky spring: A novel musical toy," in *Proc. DAFx-10*, Graz, Austria, Sept. 2010.

[12] V. Välimäki, J. Parker, and J. S Abel, "Parametric spring reverberation effect," *J. Audio Eng. Soc.*, vol. 58, no. 7/8, pp. 547–562, 2010.

[13] J. O. Smith, "Physical modeling using digital waveguides," *Computer Music Journal*, vol. 16, no. 4, pp. 74–91, 1992.

[14] V. Välimäki, J. Pakarinen, C. Erkut, and M. Karjalainen, "Discrete-time modelling of musical instruments," *Reports on Progress in Physics*, vol. 69, no. 1–78, pp. 1, 2006.

[15] S.A. Amman and M. Das, "An efficient technique for modeling and synthesis of automotive engine sounds," *IEEE Trans. Industrial Electronics*, vol. 48, no. 1, pp. 225–234, 2001.

[16] S. Cecchi, A. Primavera, L. Romoli, F. Piazza, F. Bettarelli, and A. Lattanzi, "Investigation into electric vehicles exterior noise generation," in *133rd AES Conv.*, Oct. 2012.

[17] A. Farnell, *Designing Sound*, The MIT Press, 2010.

[18] L. Peltola, C. Erkut, P.R. Cook, and V. Välimäki, "Synthesis of hand clapping sounds," *IEEE Trans. Audio, Speech, and Lang. Process.*, vol. 15, no. 3, pp. 1021–1029, 2007.

[19] P. R. Cook, *Real Sound Synthesis for Interactive Applications*, AK Peters, Ltd., 1st edition, 2002.

[20] D. Rocchesso and F. Fontana, Eds., *The Sounding Object*, Mondo Estremo, 2003.

[21] P. F. Hoffmann, F. Gosselin, and F. Taha, "Analysis of the drilling sound component from expert performance in a maxillo-facial surgery," in *Proc. ICAD2009*, Copenhagen, Denmark, May 18–21 2009.

[22] J. O. Smith, *Physical Audio Signal Processing*, http://ccrma.stanford.edu/~jos/pasp/, accessed June 17, 2013, online book.

[23] S. A. Van Duyne and J. O. Smith, "A simplified approach to modeling dispersion caused by stiffness in strings and plates," in *Proc. ICMC 1994*, Aarhus, Denmark, 1994, pp. 335–343.

[24] J. Rauhala and V. Välimäki, "Dispersion modeling in waveguide piano synthesis using tunable allpass filters," in *Proc. DAFx-2006*, Montreal, Canada, 2006, pp. 71–76.

This report summarizes the results of the KAPRI project, noise generation mechanisms of the percussive rock drilling and breaking hammer operations. At first, a literature study was conducted to find out existing knowledge on the topic.

The theory was tested in practice by conducting a series of strain wave, acoustic, and surface vibrations measurements under laboratory conditions. To gain more understanding on the vibration phenomena, computational models were developed to provide tools for the sound production modeling.

Objective was to utilize modeling techniques that have previously been used in musical instrument modeling, such as digital waveguides and dispersion filters. The modeling was divided to two main approaches namely a longitudinal and a transversal stress wave model. The research work in the project had also a separate minor research topic namely acoustical analysis of excavated tunnels in rock.

Työsuojelurahasto
Arbetarskyddsfonden
The Finnish Work Environment Fund

BUSINESS +
ECONOMY

ART +
DESIGN +
ARCHITECTURE

SCIENCE +
TECHNOLOGY

CROSSOVER

DOCTORAL
DISSERTATIONS